A computer experiment on diffusion in the Lorentz gas

C. Bruin

11-6 6110

A computer experiment on diffusion
in the Lorentz gas

A computer experiment on diffusion in the Lorentz gas

Proefschrift ter verkrijging
van de graad van doctor in de
technische wetenschappen
aan de Technische Hogeschool Delft,
op gezag van de rector magnificus
prof. ir. L. Huisman,
voor een commissie aangewezen
door het college van dekanen
te verdedigen op
woensdag 1 maart 1978
te 16.00 uur door
Cornelis Bruin
natuurkundig ingenieur
geboren te 's-Gravenhage

Delft University Press / 1978

Dit proefschrift is goedgekeurd door de promotor
prof. dr. J. M. J. van Leeuwen

Aan Tine
Ralph
Niki
Nils

CONTENTS

1. INTRODUCTION

1.1. Computer experiments

In the last two decades the use of electronic computers in statis-
tical mechanics has developed from being just a tool for computing
approximate values of configuration integrals to an alternative way of
doing experiments, or at least to a way of getting quasi-experimental
results for theoretical models.

Some noteworthy points in this development will be mentioned here.
In 1953 Metropolis et al.[1.1] computed values for the configuration
integral of a two-dimensional system of 224 hard disks by means of the
Monte Carlo method. They used a modification of the crude Monte Carlo
method, generating a Markov chain of configurations with transition
probabilities giving rise to the canonical distribution function for the
configurations in the limit of infinitely long Markov chains. The
Monte Carlo method gives only equilibrium properties, but the succession
of configurations in a Markov chain can be thought of as a quasi-kinetic
behaviour of the system. This concept is used e.g. in the kinetic Ising
model [1.2].

Soon afterwards (1956) Alder and Wainwright[1.3] introduced the
molecular-dynamics method by solving numerically the equations of motion
of systems with a hard-core interaction. They obtained in this way
static quantities (related to the equation of state) as well as time-
dependent ones as the velocity autocorrelation function.

A breakthrough to more realistic systems was made in 1964 by Rahman.
He solved the equations of motion, written as difference equations, of a
system of 864 particles with a Lennard-Jones interaction chosen to
simulate liquid argon[1.4]. He was the first to stress the relevance of
these computations for quasi-elastic neutron scattering. He computed
in this spirit apart from the velocity autocorrelation function also

the density-density correlation function in space and time. Later on, not only the self-diffusion coefficient but also bulk and shear viscosities and the heat conductivity that are much harder to calculate for such a system have been determined.[1.5] This method, suitable for systems with any interaction potential given in an analytic or tabulated form, is presently being applied for the simulation of such complicated systems like water[1.6], molten salts[1.7] and plasmas.[1.8]

As a final example, the conceptually important result is mentioned of Alder and Wainwright[1.9] in 1970, i.e. the discovery of the long-time tails of the velocity autocorrelation function.

This thesis is concerned with a molecular-dynamics study of a problem which is also mostly of a conceptual nature. In the study of the density dependence of transport coefficients Dorfman and Cohen[1.10] discovered that a power-series expansion of the transport coefficients is most likely to be impossible. Their argument is based on a phase space estimate of the integrals yielding the higher-order density corrections to the low-density (Boltzmann) values of the transport quantities. As the restriction imposed by the (irreducible) N-body dynamics on the phase space is not sufficient to guarantee the convergence of the integrals over the pertinent collision sequences, they concluded that the density series proposed so-far was divergent in sufficiently high order (depending on the dimensionality of the system).

We will show that the so-called Lorentz gas is an ideal molecular-dynamics testing ground for this issue. The Lorentz gas is a random assembly of spherical scatterers through which one spherical particle moves. The fixed scatterers are chosen to be point-particles and cannot move. Another type of Lorentz gas, the wind-tree model due to Ehrenfest, has been studied in another context by Wood and Lado[1.11];in this model a point-particle is scattered by fixed parallel squares.

The phase space of the Lorentz gas is (N + 2)d dimensional, d being the dimensionality of the system and N the number of scatterers. Since the absolute value of the momentum of the moving particle is a constant of motion, trajectories always remain on the same sphere in

momentum space. This makes integrals over momentum space trivial. The positions of the scatterers are not affected by the time evolution of the system, and therefore a Monte Carlo procedure is needed to sample their Nd-dimensional configuration space. The trajectory of the moving particle in a given configuration of the scatterers can be computed by means of molecular dynamics in a simplified version with respect to Alder and Wainwright[1.12]; there being only one moving particle with constant velocity. In this way phase space can be sampled properly if enough computing time is available and if there are no closed pockets in the generated configurations of scatterers. Such closed pockets, which are disconnected regions in the configuration space of the moving particle, can be dealt with by a Monte Carlo procedure for the generation of initial positions of the moving particle.

The computations presented here are an example of obtaining quasi-experimental results for a theoretical model that has no clear-cut analogue in nature.

1.2. Diffusion in the Lorentz gas

Transport coefficients can be calculated from equilibrium averages of time correlation functions. These functions provide also a particularly suitable starting point for the investigation of the density dependence of transport coefficients. Zwanzig[1.13] designed a simple scheme for computing the coefficients of a power-series expansion in the density for transport coefficients. However, as mentioned before, actual calculations lead to divergencies in certain expansion coefficients. Proper resummation gave rise to terms logarithmic in the density[1.14-1.17].

Although these theoretical predictions date from several years ago, there is as yet no experimental confirmation for the existence of logarithmic terms. The reason is that for real systems the coefficients of these terms are unknown and, probably, small[1.18]. This smallness is supported by the result of the explicit calculation[1.16,1.17] for the three-dimensional Lorentz gas of the coefficient of the first

logarithmic term in the density expansion for the diffusion coefficient.

For the two-dimensional Lorentz gas the coefficient of the first logarithmic term turns out to be comparatively large[1.17]. The main objective of the present study is to find confirmation for the existence of this term from combined Monte Carlo and molecular-dynamics calculations (for which the model is very well suited).

Another reason for studying the Lorentz gas is provided by Ernst and Weyland[1.19]. They derived an expression for the earlier mentioned long-time behaviour of the velocity autocorrelation function for a d-dimensional Lorentz gas at low densities. In systems with complete hydrodynamics like the hard-sphere gas the expression has a positive sign and contains an inverse power of time: $t^{-d/2}$; see refs.[1.9, 1.20], and ref[1.21]. For the Lorentz gas, where diffusion is the only hydrodynamic mode, the expression has a negative sign and a $t^{-\frac{1}{2}d-1}$ behaviour. Therefore the diffusion coefficient, which is the time integral over the velocity autocorrelation function, remains finite also in two dimensions. This asymptotic behaviour of the velocity autocorrelation function is a very small effect.

1.3. Survey

In chapter 2 theoretical considerations on the Lorentz gas are presented. In section 2.1 the Lorentz gas is defined, together with the most important quantities. In the first part of section 2.2 an outline of the expansion method is given, whereas the second part gives a summary of the calculations of van Leeuwen and Weyland for the expansion coefficients up to the first logarithmic ones both for d = 2 and d = 3. In sub-section 2.2.3 the diagrams giving a regular contribution to the same order in the density as the first logarithmic term are listed together with their contributions for the two-dimensional case. The numerical computations are discussed briefly. In sub-section 2.2.4 the diagrams contributing to the squared logarithmic term, one order higher in the density, are listed together with their contributions, which could be obtained analytically. In sub-section 2.2.5 the Boltzmann expressions

are given for the velocity autocorrelation function as well as the expressions for asymtotic long times found by Ernst and Weyland.

In section 2.3 expressions are derived for the free-time distribution and the mean free time. These quantities have been chosen as a test on the randomness of the scatterers and they serve the purpose rather well. The distribution of first free times is purely exponential but the free-time distribution (including second, third, etc. free times as well) must be handled with care. It turns out to be essential in what way one takes averages over the results of different configurations. In the appendix an explicit calculation is given, for the two-dimensional case, of the joint distribution of the first and second free time, leading to a non-exponential behaviour for the distribution of second free times. The chapter closes with some considerations on finite-size effects.

The method of computation is explained in chapter 3, starting with the crude Monte Carlo method for generating different configurations of scatterers. In section 3.2 the computation of trajectories by means of molecular dynamics is described. In the next section different ways of obtaining the velocity autocorrelation function and the mean square displacement are discussed. The computational method for obtaining the diffusion coefficient from these functions is given in section 3.4. The computation of the mean free time and distribution of free times is dealt with in section 3.5, where the different ways of taking averages are emphasized.

In chapter 4 the computer results are presented on the mean free time, the distribution of free times, the velocity autocorrelation function, the mean-square displacement and the diffusion coefficient.

In chapter 5 the conclusions are summarized.

References

1.1) Metropolis, N., et al., J. Chem. Phys. 21 (1953) 1087

1.2) Compagner, A., J. Phys. Soc. Japan Suppl. 26 (1969) 229
Stoll, E., Binder, K. and Schneider, T., Phys. Rev. B8 (1973) 3266

1.3) Alder, B.J. and Wainwright, T.E., (1956) in Internat. Symp. on
Stat. Mech. Theory of Transport Processes. Ed. I. Progogine,
Interscience, Brussels 1958

1.4) Rahman, A., Phys. Rev. 136 (1964) A405

1.5) Bruin, C., Phys. Letters 28A (1969) 777

1.6) Rahman, A. and Stillinger, F.H., J. Chem. Phys. 55 (1971) 3336

1.7) Hansen, J.P. and McDonald, I.R., J. Phys. C 7 (1974) L384

1.8) Hockney, R.W., Goel, S.P. and Eastwood, J.W., Chem. Phys. Letters 21
(1973) 589

1.9. Alder, B.J. and Wainwright, T.E., Phys. Rev. A1 (1970) 18

1.10) Dorfman, J.R. and Cohen, E.G.D., Phys. Letters 16 (1965) 124

1.11) Wood, W.W. and Lado, F., J. Comp. Phys. 7 (1971) 528

1.12) Alder, B.J. and Wainwright, T.E., J. Chem. Phys. 31 (1959) 459

1.13) Zwanzig, R., Phys. Rev. 129 (1963) 486

1.14) Sengers, J.V., Phys. Rev. Letters 15 (1965) 515

1.15) Haines, L.K., Dorfman, J.R. and Ernst, M.H., Phys. Rev. 144
(1966) 207

1.16) Van Leeuwen, J.M.J. and Weyland, A., Physica 36 (1967) 457

1.17) Weyland, A. and Van Leeuwen, J.M.J., Physica 38 (1968) 35

1.18) Kestin, J., Paykoç, E. and Sengers, J.V., Physica 54 (1971) 1

1.19) Ernst, M.H. and Weyland, A., Phys. Letters 34A (1971) 39

1.20) Ernst, M.H., Hauge, E.H. and Van Leeuwen, J.M.J., Phys. Rev. Letters 25 (1970) 1254

1.21) Dorfman, J.R. and Cohen, E.G.D., Phys. Rev. Letters 25 (1970) 1257

2. THEORY

2.1. Definition of the model

The essential feature of a Lorentz gas is that only one particle moves in an assembly of static particles. In the classical case one has for the Hamilton function

$$H(x,R^N) = \frac{p^2}{2m} + \sum_{j=1}^{N} V_{dy}(\vec{q} - \vec{R}_j) + \frac{1}{2!} \sum_{i \neq j} V_{st}(\vec{R}_i - \vec{R}_j) , \qquad (2.1)$$

where x stands for $(\vec{p},\vec{q})$, $\vec{q}$ is the position and $\vec{p} = m\vec{v}$ the momentum of the moving particle, m being its mass and $\vec{v}$ its velocity. The coordinates of the N static particles are denoted by $R^N = (\vec{R}_1, \ldots, \vec{R}_N)$. For the dynamical part of the interaction $V_{dy}(\vec{q} - \vec{R}_j)$, operating between the moving particle and scatterer j, we take a spherically symmetric hard-core potential

$$V_{dy}(\vec{q} - \vec{R}_j) = \begin{cases} \infty & \text{for } |\vec{q} - \vec{R}_j| \leq \sigma , \\ \\ 0 & \text{for } |\vec{q} - \vec{R}_j| > \sigma . \end{cases} \qquad (2.2)$$

Similarly, for the interaction $V_{st}(\vec{R}_i - \vec{R}_j)$ between two scatterers we take

$$V_{st}(\vec{R}_i - \vec{R}_j) = \begin{cases} \infty & \text{for } |\vec{R}_i - \vec{R}_j| \leq \sigma_s , \\ \\ 0 & \text{for } |\vec{R}_i - \vec{R}_j| > \sigma_s . \end{cases} \qquad (2.3)$$

Furthermore we will assume the scatterers to be point-particles, $\sigma_s = 0$, so the third term in (2.1) is zero.

With these specifications our model is a system of N point-scatterers

between which a single sphere of radius σ is moving. Alternatively the model can be looked at as being a system of N possibly overlapping scatterers of radius σ with one moving point-particle. The system is enclosed in a d-dimensional box of volume Ω. Instead of the density of scatterers $n = N/\Omega$, the reduced density $n^* = n\sigma^d$ will be used, which is dimensionless. Strictly speaking, it is necessary for the analysis below to take the thermodynamic limit ($N \to \infty$ and $\Omega \to \infty$, keeping n fixed).

The diffusion coefficient of the moving particle is the quantity of most interest in this study. The relation between the diffusion co-efficient D_T at a certain temperature T and the velocity autocorrelation function reads

$$D_T = \frac{1}{d} \int_0^\infty dt \ <\vec{v}(0) . \vec{v}(t)>_T \ , \tag{2.4}$$

where $\vec{v}(t)$ denotes the velocity of the moving particle at time t and the average $<..>_T$ is a canonical average over all distributions of the scatterers and of the moving particle (with temperature T). One can write (2.4) in more detail,

$$D_T = \frac{1}{d} \int_0^\infty dt \int dx \int dR^N \ \rho(x,R^N) \ \vec{v}. \ \{exp \ tL(x,R^N)\} \ \vec{v} \ , \tag{2.5}$$

making use of the Liouville operator $L(x,R^N)$ defined by

$$\{exp \ tL(x,R^N)\} \ x = x(t), \quad x(0) = x \ , \tag{2.6}$$

and the canonical distribution function given by

$$\rho(x,R^N) = \{exp \ -\beta H(x,R^N)\}/\int dx \int dR^N \ exp \ -\beta H(x,R^N) \ , \tag{2.7}$$

with $\beta = 1/kT$, k being Boltzmann's constant.

The absolute value v of the velocity of the moving particle is a constant of motion. Therefore the average over the Maxwell-Boltzmann distribution $\varphi_T(\vec{v})$, needed to obtain results at a given temperature T, does not interfere with the spatial averages. Denoting by $<..>$ the

average over the spatial coordinates only, we find for the average at fixed temperature T:

$$\langle \vec{v}(0) \cdot \vec{v}(t) \rangle_T = \int d\vec{v} \; \varphi_T(\vec{v}) \; \langle \vec{v}(0) \cdot \vec{v}(t) \rangle \; , \tag{2.8}$$

where in the average on the right-hand side the absolute value v of the velocity of the moving particle is kept fixed. Apart from a trivial factor v^2, the velocity dependence of $\langle \vec{v}(0) \cdot \vec{v}(t) \rangle$ appears only in the form of a scale factor in the time dependence. Thus we may write

$$\langle \vec{v}(0) \cdot \vec{v}(t) \rangle = v^2 \; \psi(vt/\sigma) \; , \tag{2.9}$$

where a factor σ is included to define a reduced time

$$t^* = vt/\sigma \; . \tag{2.10}$$

Inserting (2.8) and (2.9) into (2.4) and using t^* as an integration variable one finds

$$D_T = \frac{\Gamma(\frac{1}{2}d + \frac{1}{2})}{\Gamma(\frac{1}{2}d + 1)} \left[\frac{kT}{2m} \right]^{\frac{1}{2}} \sigma \int_0^\infty dt^* \; \psi(t^*) \; . \tag{2.11}$$

For our purpose it is more convenient to use a diffusion coefficient D for a fixed velocity v, for which one easily obtains

$$D = \frac{1}{d} \int_0^\infty dt \; \langle \vec{v}(0) \cdot \vec{v}(t) \rangle = \frac{v\sigma}{d} \int_0^\infty dt^* \; \psi(t^*) \; . \tag{2.12}$$

Another useful scaling quantity is the Boltzmann mean free time τ, which will be discussed in detail in section 2.3. Since the scatterers are point-particles the collision rate Γ, the number of collisions per unit time, is easily calculated. One obtains for its inverse, the reduced mean free time $\tau^* = v\tau/\sigma$, the expression

$$\tau^* = 1/a_d n^* \; , \tag{2.13}$$

where a_d is the reduced cross section, given by $a_1 = 1$, $a_2 = 2$ and $a_3 = \pi$. Defining a reduced time $s = t^*/\tau^*$ and subsequently a reduced velocity autocorrelation function $\phi(s) = \psi(t^*)$, we find from (2.12) the reduced diffusion coefficient

$$D/v\sigma = \frac{\tau^*}{d} \int_0^\infty ds\ \phi(s) \quad . \tag{2.14}$$

From a numerical point of view it may be convenient to calculate alternatively the diffusion coefficient from the slope of the mean square displacement at long times:

$$D/v\sigma = \lim_{s \to \infty} \frac{\tau^*}{2d} \frac{d\Delta(s)}{ds} \quad , \tag{2.15}$$

where

$$\Delta(s) = <[\vec{q}(s) - \vec{q}(0)]^2>/\sigma^2 \quad , \tag{2.16}$$

$\vec{q}(s)$ being the position of the moving particle at time s.

2.2. Density expansion

2.2.1. *Outline of the expansion method*

The scheme for the density expansion of the diffusion coefficient (or rather of its inverse) has been given in detail by Van Leeuwen and Weyland[2.1) for the two- and three-dimensional Lorentz gas of spherical particles. It can be summarized as follows. First one performs an Ursell expansion on the time-evolution operator $\exp tL(x,R^N)$ in eq. (2.5). This already gives a density expansion for the velocity autocorrelation function

$$\psi(t^*) = 1 + \sum_{\ell=1}^\infty n^{*\ell} \tilde{\beta}_\ell(t^*) \quad , \tag{2.17}$$

where the coefficient $\overset{\sim}{\beta}_\ell(t^*)$ denotes the contribution of the ℓ-particle Ursell operator. Unfortunately, the coefficient $\overset{\sim}{\beta}_\ell(t^*)$ increases with time as $t^{*\,\ell}$. Therefore the time integral over these terms diverges for $t^* \to \infty$. This is not surprising, since a density expansion for the diffusion coefficient itself does not exist, the diffusion coefficient becoming larger and larger the more dilute the system of scatterers is. Therefore one should rather aim at a density expansion for the inverse diffusion coefficient.

For that purpose it is convenient to study the Laplace transform $\hat{\psi}(z^*)$ of the velocity autocorrelation function $\psi(t^*)$:

$$\hat{\psi}(z^*) = \int_0^\infty e^{-z^* t^*} \psi(t^*) \, dt^* \quad . \tag{2.18}$$

According to (2.12) D/vσ is related to $\hat{\psi}(z^*)$ as

$$D/v\sigma = \lim_{z^* \to 0} \frac{1}{d} \hat{\psi}(z^*) \quad , \tag{2.19}$$

where we have deliberately used the limit $z^* \to 0$ notation in order to deal with anticipated long-time divergencies, which demonstrate themselves in singular small z^* behaviour. From (2.5) and (2.19) the following formal expression for $\hat{\psi}(z^*)$ can be obtained:

$$\hat{\psi}(z^*) = v^{-2} \int d\vec{q} \int dR^N \, \rho(\vec{q}, R^N) \, \vec{v} \cdot [z - L(x, R^N)]^{-1} \vec{v} \quad , \tag{2.20}$$

where $\rho(\vec{q}, R^N)$ is the microcanonical distribution function, which is suitable for obtaining spatial averages at fixed v. The Laplace variable z conjugated to t is $z = z^* v/\sigma$. In the extreme dilute limit one has $L(x, R^N) \, \vec{v} \approx \vec{v}$ and therefore $\hat{\psi}(z^*)$ diverges as z^{*-1}. Thus $\hat{\psi}(z^*)$ is written as

$$\hat{\psi}(z^*) = [z^* + \gamma(z^*)]^{-1} \quad , \tag{2.21}$$

where $\gamma(z^*)$ incorporates the collision effects.

This quantity $\gamma(z^*)$ can be expanded in the density,

$$\gamma(z^*) = \sum_{\ell=1}^{\infty} n^{*\ell} \gamma_\ell(z^*) \ . \tag{2.22}$$

A complete treatment[2.1)] gives for the first few $\gamma_\ell(z^*)$ the following re-sults:

$$\gamma_1(z^*) = - z \ \beta_1(z^*)$$
$$\gamma_2(z^*) = - z \ [\ \beta_2(z^*) - \beta_1^2(z^*)]$$
$$\gamma_3(z^*) = - z \ [\ \beta_3(z^*) - 2\beta_2(z^*) \ \beta_1(z^*) + \beta_1^3(z^*)] \ . \tag{2.23}$$

The function $\beta_\ell(z^*)$ is related to the ℓ-particle Ursell operator, being equal to the product of the Laplace transform of $\overset{\gamma}{\beta}_\ell(t^*)$ (2.17) and a factor $z - L(x)$, where $L(x)$ is the Liouville operator in the case of free streaming.

The original hope was that the $\gamma_\ell(z^*)$ would behave well for $z^* \to 0$ such that eq. (2.22) implies a series expansion for $v\sigma/D$. The earlier mentioned divergencies $\sim t^{*\ell}$ exhibit themselves as singularities $\sim z^{*-\ell}$ in the $\beta_\ell(z^*)$. As (2.23) indicates, the relation between $\gamma_\ell(z^*)$ and the $\beta_\ell(z^*)$ is such that the dominant singularities are subtracted and then $\gamma_\ell(z^*)$ possibly stays finite for $z^* \to 0$. Thus one would obtain a power series

$$v\sigma/D = \sum_{\ell=1}^{\infty} n^{*\ell} \gamma_\ell(0) \ . \tag{2.24}$$

However, this subtraction mechanism does not work, since also other singularities than the dominant ones occur. As will be shown in the following sections, the density expansion turns out to be in two dimensions

$$v\sigma/D = c_1 n^* + c_2' n^{*2} \ln n^* + c_2 n^{*2} + c_3'' n^{*3} (\ln n^*)^2 + \ldots \tag{2.25}$$

with

$$c_1 = \frac{16}{3}, \quad c_2' = -\frac{64}{9}, \quad c_2 = -4.68, \quad c_3'' = 24.10, \qquad (2.26)$$

and in three dimensions

$$v\sigma/D = b_1 n^* + b_2 n^{*2} + b_3' n^{*3} \ln n^* + \dots \qquad (2.27)$$

with

$$b_1 = 3\pi, \quad b_2 = 19.05, \quad b_3' = 0.645. \qquad (2.28)$$

2.2.2. *First few expansion coefficients*

The calculation of c_1, c_2', b_1, b_2 and b_3' will now be outlined, as performed by Van Leeuwen and Weyland[2.1, 2.2]. The function $\beta_\ell(z^*)$, introduced in (2.23), is defined in terms of the usual reduced density distribution function $g(\vec{q}, R^\ell)$ and the collision operator $B_z(x, R^\ell)$ as

$$\beta_\ell(z^*) = \sigma^{-\ell} d \frac{\vec{v}}{v^2} \cdot \int \frac{dR^\ell}{\ell!} \; g(\vec{q}, R^\ell) \; B_z(x, R^\ell) \; \vec{v}, \qquad (2.29)$$

where $B_z(x, R^\ell)$ is proportional to the Laplace transform of the Ursell operator of the moving particle and ℓ scatterers. To give an example, the so-called binary kernel $B_z(x, \vec{R}_i)$, which involves only one scatterer, is defined as

$$B_z(x, \vec{R}_i) = \int_0^\infty dt \; e^{-zt} \; [\exp tL(x, \vec{R}_i) - \exp tL(x)] \; [z - L(x)]. \qquad (2.30)$$

Two contributions can be recognized in the binary kernel $B_z(x, \vec{R}_i)$: one due to a real collision, $B_z^r(x, \vec{R}_i)$, corresponding to the two-particle operator $\exp tL(x, \vec{R}_i)$, and the other due to a virtual collision, $B_z^v(x, R_i)$, corresponding to the free streaming operator $\exp tL(x)$. One

has obviously

$$B_z(x,\vec{R}_i) = B_z^r(x,\vec{R}_i) - B_z^v(x,\vec{R}_i) \ . \tag{2.31}$$

To evaluate the coefficients $\gamma_\ell(z^*)$ it is necessary, for $\ell \geqslant 2$, to introduce the binary collision expansion. By this expansion $B_z(x,R^\ell)$ is expressed as an iterated sum over products of the binary kernel, $B_z(x,\vec{R}_i)$. This means that the generated collision sequences are characterized by the number of collisions that the moving particle suffers from a certain number of scatterers. One has in particular for $\beta_2(z^*)$:

$$\beta_2(z^*) = \sum_{j=2}^{\infty} \beta_{2,j}(z^*) \ , \tag{2.32}$$

where in $\beta_{2,j}(z^*)$ the first subscript denotes the number of scatterers involved and the second one the number of binary kernels, i.e. the number of collisions.

Furthermore it is useful to divide the contributions in 'dynamical' and 'statistical' ones:

$$\beta_\ell(z^*) = \beta_\ell^{dy}(z^*) + \beta_\ell^{st}(z^*) \ , \tag{2.33}$$

with the definitions

$$\beta_\ell^{dy}(z^*) = \sigma^{-\ell d} \frac{\vec{v}}{v^2} \cdot \int \frac{dR^\ell}{\ell!} \ B_z(x,R^\ell)\vec{v}$$

$$\beta_\ell^{st}(z^*) = \sigma^{-\ell d} \frac{\vec{v}}{v^2} \cdot \int \frac{dR^\ell}{\ell!} [\, g(\vec{q},R^\ell) - 1]\ B_z(x,R^\ell)\vec{v} \ . \tag{2.34}$$

The statistical (more complicated) part is defined such that it is zero for large distances between the particles. The motivation for this division is that possible divergencies can only originate from contributions at asymptotically large distances and therefore will occur dominantly in the (relatively simple) dynamical part.

For the calculation of $\gamma_1(z^*)$, see (2.23), there is no need for the binary collision expansion. In the limit of $z^* \to 0$ there is no contri-

bution from $\beta_1^{st}(z^*)$, since this quantity remains finite in this limit due to the factor $[g(\vec{q},\vec{R}) - 1]$ which is zero for large distances. The dynamical part $\beta_1^{dy}(z^*)$ is easily evaluated and substitution in (2.23) leads to

$$\gamma_1^{dy}(z^*) = \begin{cases} 8/3 & \text{for } d = 2 \ , \\ \\ \pi & \text{for } d = 3 \ . \end{cases} \tag{2.35}$$

Inspecting the expression (2.23) for $\gamma_2(z^*)$, we observe that contributions arise from both $\beta_1(z^*)$ and $\beta_2(z^*)$. The first contribution $\beta_{2,2}^{dy}(z^*)$, the dynamical two-scatterers two-collisions contribution, has the property

$$\beta_{2,2}^{dy}(z^*) = [\beta_1^{dy}(z^*)]^2 \ , \tag{2.36}$$

because the two collisions occur at two independent scatterers (and no statistics is involved). Therefore both the singular terms of (2.36) cancel in (2.23), as was indicated in the last section. The first non-vanishing collision sequence appears through $\beta_{2,3}^{dy}(z^*)$, where the moving particle collides with a first scatterer, then with a second scatterer and again with the first one (see fig. 2.1). This process is divergent in
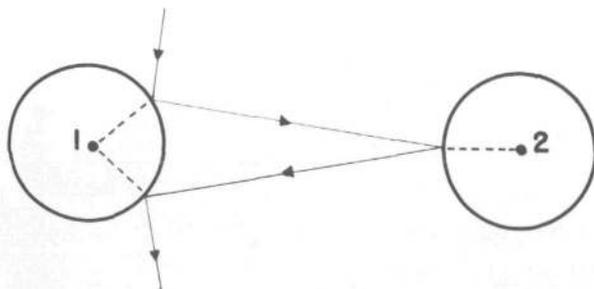

Fig. 2.1. *Collision sequence corresponding to* $\beta_{2,3}^{dy}(z^*)$*, the first and the last collision chosen to be real.*

the two-dimensional case for $z^* \to 0$ and leads to

$$\gamma_{2,3}^{dy}(z^*) = -\frac{1}{2} \left(\frac{8}{3}\right)^2 \ln z^* + O(1) \quad \text{for } d = 2 \quad . \tag{2.37}$$

The second suffix of $\gamma_{\ell,j}(z^*)$ has the same meaning as the one of $\beta_{\ell,j}(z^*)$ (2.32) and counts the number of binary collision operators involved in the diagram.

In order to convert the power series in the density n^*, which diverges with $z^* \to 0$, into a convergent series, one performs a renormalization summation. In the case mentioned above, $\gamma_{2,3}^{dy}(z^*)$, which is the lowest order ring diagram, one sums over all the higher-order ring diagrams $\gamma_{\ell,\ell+1}(z^*)$ and obtains the so-called ring sum $\gamma_r(z^*)$:

$$\gamma_r(z^*) = \sum_{\ell=2}^{\infty} n^{*\ell} \, \gamma_{\ell,\ell+1}^{dy}(z^*) \quad . \tag{2.38}$$

This sum is hard to do in general, but fortunately the main interest is in the $n^* \to 0$ behaviour. As a general guide-line for renormalization, which is also of computational value, one can use the following receipt. Take a diagram, e.g. $\gamma_{2,3}^{dy}(z^*)$, where all collisions are real ($B_z^r(x,\vec{R}_i)$), except the first and the last one ($B_z(x,\vec{R}_i)$), and dress it with all possible virtual collisions ($B_z^v(x,\vec{R}_i)$). As a first approximation the contribution of such a sum is obtained by replacing the parameter z^* by $z^* + a_d n^*$ (see (2.13) for the definition of a_d). Then one may take the limit $z^* \to 0$ and one sees that a $\ln z^*$ in the unrenormalized contribution is replaced by a $\ln n^*$ in the renormalized diagram contribution, called $\gamma_{2,3}^{r,dy}(z^*)$. Along these lines the regular contributions can also be obtained, though often with considerable more effort. Weyland and Van Leeuwen[2.2] obtained for the ring sum $\gamma_r(z^*)$ in this way

$$\gamma_r(0) = -\frac{1}{2} \left(\frac{8}{3}\right)^2 n^{*2} \ln n^* + O(n^{*2}) \quad \text{for } d = 2 \quad . \tag{2.39}$$

In the three-dimensional case $\gamma_2(z^*)$ is finite. Of the dynamical terms only $\gamma_{2,3}^{dy}(0)$ and $\gamma_{2,4}^{dy}(0)$ have been evaluated:

$$\gamma_{2,3}^{dy}(0) = \pi^2 \ (1/3 + 4\pi^2/105)$$

$$\text{for } d = 3 \ . \tag{2.40}$$

$$\gamma_{2,4}^{dy}(0) = -0.65 \pm 0.01$$

Because of the rapid decrease in the contributions of diagrams with an increasing number of collisions and the same number of scatterers[2.2], it was argued by Van Leeuwen and Weyland that the contribution from higher-order terms would only amount to a few percent. The statistical terms are all zero to lowest order in the density for our case of point-scatterers.

The calculation of $\gamma_3(z^*)$ does yield a divergent result in three dimensions. The responsible diagrams are $\gamma_{3,4}^{dy}(z^*)$ and $\gamma_{3,5}^{dy}(z^*)$. Their contributions amount to

$$\gamma_{3,4}^{dy}(z^*) = \frac{\pi^3}{4} \ \ln z^* + 0(1),$$

$$\text{for } d = 3 \ . \tag{2.41}$$

$$\gamma_{3,5}^{dy}(z^*) = -[\pi^3/4 - 0.215] \ \ln z^* + 0(1)$$

It is clear from (2.41) that it will not suffice to sum over the ring diagrams $\gamma_r(z^*)$ only to remove these divergencies, but that one also has to sum over a special class of diagrams $\gamma_s(z^*)$ corresponding to $\gamma_{3,5}^{dy}(z^*)$. The result of these sums reads

$$\gamma_r(0) + \gamma_s(0) = 0.215 \ n^{*3} \ \ln n^* + 0(n^{*3}) \ . \tag{2.42}$$

2.2.3. Higher-order regular contributions in two dimensions

For the comparison of the computer-experiment results with the diffusion coefficient obtained from the density expansion, which comparison will be performed mainly for the two-dimensional case, it is convenient to know the contributions from terms next to the first singular one. In this section the diagrams of order n^{*2} will be discussed and their contributions will be given. There are four sources

of regular contributions of order n^{*2}:

1) $\displaystyle\lim_{n^* \to 0} \gamma_{2,3}^{r,dy}(0)_{regular} = -3.572,$

2) $\displaystyle\lim_{n^* \to 0} \sum_{\ell=3}^{\infty} n^{*(\ell-2)} \gamma_{\ell,\ell+1}^{r,dy}(0) = 1.020,$

3) $\displaystyle\sum_{\ell=4}^{\infty} \gamma_{2,\ell}^{dy}(0) = -1.92,$

4) $\displaystyle\lim_{n^* \to 0} \sum_{\ell=1}^{\infty} n^{*\ell} \gamma_{2+\ell,3+\ell}^{r,v}(0) = 2.13.$

$$(2.43)$$

Ad 1) This contribution results from a more complete calculation of a part of the ring sum $\gamma_r(0)$, see (2.38) and (2.39). The logarithmic term in (2.39) is due to the renormalized diagram $\gamma_{2,3}^{r,dy}(0)$. This renormalized diagram also gives a regular contribution of order n^{*2}, in the low-density limit. The calculation is complicated and contains a series expansion in terms of Bessel functions. The first term in this expansion can be obtained analytically and yields the logarithmic term and a regular contribution. The other terms in this expansion, all regular, have to be computed numerically. The series converges fast. The first seven terms have been computed to obtain the above mentioned result, the next six terms would contribute by an amount of the order of 10^{-4}.

Ad 2) The other part of the ring sum contains renormalized ring diagrams of higher order, $\gamma_{\ell,\ell+1}^{r,dy}$ with $\ell \geqslant 3$. At first sight it may be surprising that diagrams with more than two scatterers do contribute to order n^{*2}. Indeed the unrenormalized diagrams $\gamma_{\ell,\ell+1}^{dy}$ contribute to order $n^{*\ell}$, but the renormalization leads to cancellation of $\ell - 2$ powers of the density. For the calculation it is convenient to split the sum over the higher-order ring diagrams into two parts. One sum converges slowly, but fortunately can be done analytically, giving a contribution of $64(\frac{1}{2} - 1/\pi)/9$. The other sum converges rapidly, successive terms decreasing by about a factor of ten. The result obtained is: -0.2724 ± 0.00005.

Ad 3) This infinite number of diagrams, $\gamma_{2,\ell}^{dy}(0)$, for $\ell \geqslant 4$, is generated by the binary collision expansion, see (2.32). Together they

represent all possible collision sequences between the moving particle
and two scatterers only, with the total number of collisions ≥ 4. They
give a non-zero contribution only when all the collisions are real, ex-
cept the first and the last collision. No diagram could be reduced further
than to a three-dimensional integral. These integrals have been computed
numerically. For even ℓ the diagrams appear to give negative and for odd
ℓ positive contributions. After 20 terms the absolute value of the terms
is reduced to 0.1% of the first term. The sum of two succeeding terms,
of opposite sign, is even smaller. The sum of terms between 20 and 40
indeed appears to be negligible. The succeeding ones will be even more so,
especially because the accuracy of the numerical integration of the first
terms is not much better than one percent.

Ad 4) This last contribution of order n^{*2} comes from a class of dia-
grams closely related to the renormalized diagram $\gamma_{2,3}^{r,dy}$. In the renorma-
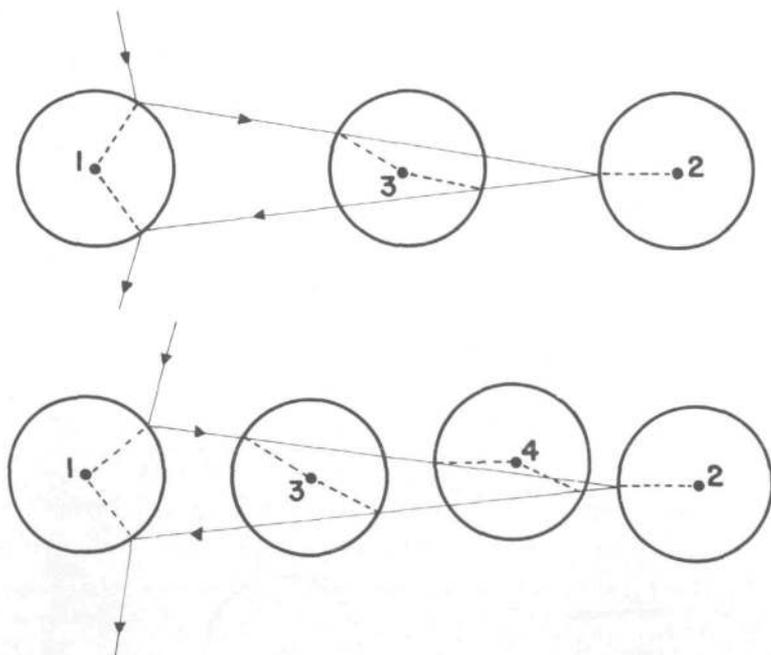

Fig. 2.2. Two diagrams of the special class, the first and the last
   collisions chosen to be real.

lization procedure diagrams are 'dressed' with an arbitrary number of intermediate scatterers, undergoing virtual collisions only. It has been argued by Weyland and Van Leeuwen[2.2) that the ring diagram $\gamma_{2,3}^{r,dy}$ supplied with intermediate scatterers hit twice virtually gives rise to a special class contributing in qualitatively the same way as $\gamma_{2,3}^{r,dy}$ itself. The two most simple diagrams out of this special class are shown in fig. 2.2. Taking $\gamma_{2,3}^{r,dy}$ and the special class together one arrives at the same logarithmic term as given in (2.39). The regular contribution of the special class is easily obtained from the numerical integration of a two-dimensional integral.

2.2.4. Higher-order singular contributions in two dimensions

The most divergent part of $\gamma_3(0)$, which gives rise to $\frac{1}{2}c_3''(\ln n^*)^2$ in the low-density limit after renormalization, consists of quite a number of diagrams. They are listed together with their respective contributions in table 2.1. The first diagram in table 2.1 is shown in fig. 2.3 as an example. Similarly to (2.37) only the 'dynamical' part of the diagrams lead to a density dependence of this kind. It should be noted that B_i is a short-hand notation for $B_z(x,\vec{R}_i)$. The binary collision operator $B_z(x,\vec{R}_i)$ is defined in (2.30) and its real and virtual parts, $B_z^r(x,\vec{R}_i)$ and $B_z^v(x,\vec{R}_i)$, in (2.31).
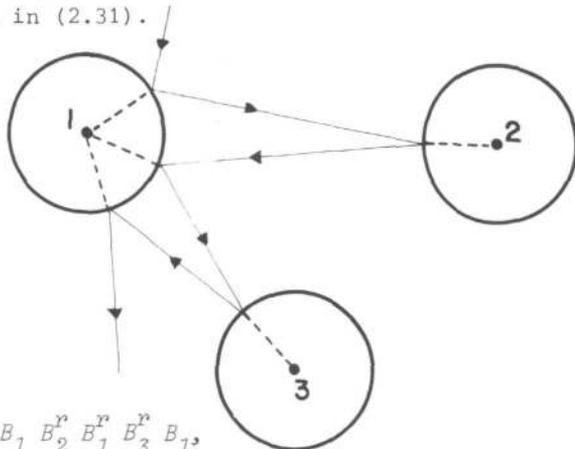
Fig. 2.3. The diagram $B_1 B_2^r B_1^r B_3^r B_1$, the first and the last collision chosen to be real.

Diagram	Contribution
$B_1\ B_2^r\ B_1^r\ B_3^r\ B_1$	$(4/3)^2\ [\ (8/3)\ -\ 2]$
$B_1\ B_2^r\ B_1^v\ B_3^r\ B_1$	$(4/3)^2\ 2$
$B_1\ B_2^r\ B_3^r\ B_1^r\ B_3$	$(4/3)^2\ 1/3$
$B_1\ B_2^r\ B_1^r\ B_3^r\ B_2$	$(4/3)^2\ 1/3$
$B_1\ B_2^r\ B_3^r\ B_1^r\ B_2$	$-(4/3)^2\ 1/2$
$B_1\ B_2^r\ B_3^r\ B_2^r\ B_1$	$(4/3)^2\ \pi/2$
$B_1\ B_2^v\ B_3^r\ B_2^r\ B_1$	0
$B_1\ B_2^r\ B_3^r\ B_2^v\ B_1$	0
$B_1\ B_2^r\ B_3^v\ B_1^r\ B_3$	$(4/3)^2$
$B_1\ B_2^r\ B_1^v\ B_3^r\ B_2$	$(4/3)^2$
$B_1\ B_2^r\ B_3^r\ B_1^v\ B_2$	$(4/3)^2$
$B_1\ B_2^v\ B_3^r\ B_1^r\ B_2$	$(4/3)^2$
$B_1\ B_2^v\ B_3^r\ B_2^v\ B_1^r\ B_2$	$(4/3)^2\ [\ 3/16\ -\ 1]$
$B_1\ B_2^r\ B_1^v\ B_3^r\ B_1^v\ B_2$	$(4/3)^2\ [\ 3/16\ -\ 1]$

Table 2.1. Diagrams contributing to $\frac{1}{2}c_3''(\ln n^*)^2$.

2.2.5. *Velocity autocorrelation function*

For the analysis of the velocity autocorrelation function it is convenient to have an expression correct to lowest order in the density, the Boltzmann approximation. This can be easily obtained by substituting (2.35) into (2.21), leading to

$$
\psi_B(t^*) = \begin{cases} \exp\left(- 8\, n^* t^*/3\right) & \text{for } d = 2 \\[2ex] \exp\left(- \pi\, n^* t^*\right) & \text{for } d = 3 \ . \end{cases} \tag{2.44}
$$

Reducing the time t^* with respect to the Boltzmann mean free time τ^*, this gives

$$
\phi_B(s) = \begin{cases} \exp - 4s/3 & \text{for } d = 2 \\[2ex] \exp - s & \text{for } d = 3 \ . \end{cases} \tag{2.45}
$$

The main interest in the velocity autocorrelation function itself lies in its behaviour for long times. On the basis of kinetic theory Ernst and Weyland[2.3] derived the asymptotic behaviour of the velocity autocorrelation function for long times:

$$
\phi_A(s) = \begin{cases} - n^*/\pi\, s^2 & \text{for } d = 2 \\[2ex] - (3\pi)^{\frac{3}{2}}\, n^{*2}/16 s^{\frac{5}{2}} & \text{for } d = 3 \ . \end{cases} \tag{2.46}
$$

The results hold to lowest order in the density and originate from the ring diagrams (which go beyond the Boltzmann approximation). They differ from the results for fluids with moving particles only ($\phi_A(s) \sim s^{-d/2}$) by the fact that the long-time tail has a negative sign and contains an additional factor s^{-1}. This also means that it will be possible to inte-

grate the velocity autocorrelation function up to the infinitely long
times, in order to obtain the diffusion coefficient.

2.3. Free-time distribution

The subject of this section is not essential for the main objective
of this thesis: the density dependence of diffusion. Apart from the fact
that the Boltzmann mean free time is a useful scaling quantity, the cal-
culation of the distribution of free times and the mean free time has
been undertaken to provide a check on the machine calculations. Initially
it was thought that the free-time distribution could be calculated exact-
ly[2.4]. However, the experimental result turns out to differ from the
theoretical result. As will be shown in this section, this can be attri-
buted to complications in the theoretical concepts involved.

For the first free time, the distribution and the mean can be
easily derived. The first free time $t_1(x,R^N)$ is defined as the time
until the first collision takes place in a configuration of N scatterers
R^N, the initial position and momentum of the moving particle being spe-
cified by $x = (\vec{p},\vec{q})$. The probability density $P_N(t)$ for finding a $t_1 = t$
is easily expressed in terms of the Dirac δ-function:

$$P_N(t) = < \delta \{t_1(x,R^N) - t\} >_{x,R^N} \quad , \tag{2.47}$$

where the average has to be taken over all allowed points in phase space
on the energy surface corresponding to velocity v. It is convenient for the
derivation to introduce the quantity

$$A_N(t) = \int_t^\infty P_N(t') \, dt' \quad , \tag{2.48}$$

which is a measure for finding a $t_1 > t$. Performing the time integral in
(2.48) after substitution of (2.47) and writing the ensemble average
explicitly one has

$$A_N(t) = \int..\int_v dx dR^N \, H\{t_1(x,R^N) - t\} \, / \, \int..\int_v dx dR^N \quad , \qquad (2.49)$$

where H is the Heaviside function ($H(t) = 0$ for $t < 0$, $H(t) = 1$ for $t \geqslant 0$) and the subscript v denotes that the integration over velocity space has to be performed at constant v. The integrand in the numerator is only different from zero when none of the scatterers is in a volume of base $a_d\sigma^{d-1}$ and height vt attached to the moving particle (again: $a_1 = 1$, $a_2 = 2$ and $a_3 = \pi$). If the volume of the moving particle Ω_m ($\Omega_m = 2\sigma$ for $d = 1$, $\Omega_m = \pi\sigma^2$ for $d = 2$ and $\Omega_m = 4\pi\sigma^3/3$ for $d = 3$) is taken into account by introducing a corrected volume $\Omega' = \Omega - \Omega_m$, one obtains by performing the integrations

$$A_N(t) = (\Omega' - vta_d\sigma^{d-1})^N \, / \, \Omega'^N \quad . \qquad (2.50)$$

Using the Boltzmann mean free time $\tau = (nva_d\sigma^{d-1})^{-1}$ or rather the Boltzmann mean free time for a system of N scatterers

$$\tau_N = \tau(1 - n\Omega_m/N) \quad , \qquad (2.51)$$

eq. (2.50) can be rewritten as

$$A_N(t) = (1 - t/\tau_N N)^N \quad . \qquad (2.52)$$

By differentiation $P_N(t)$ is obtained

$$P_N(t) = \tau_N^{-1} \, (1 - t/\tau_N N)^{N-1} \qquad (2.53)$$

and in the limit of an infinite system one has

$$P(t) \equiv \lim_{N \to \infty} P_N(t) = \tau^{-1} \exp(-t/\tau) \quad . \qquad (2.54)$$

By taking the first moment of this distribution function one finds that the average of the first free time is equal to the Boltzmann mean free time:

$$\lim_{N \to \infty} \langle t_1 \rangle_{x,R^N} = \tau \ .$$

(2.55)

For the distribution of free times, considering now the free times after the first one as well, the situation is more complicated. For the one-dimensional case Wood[2.5] derived an explicit expression for the distribution of free times. This is not a pure exponential and the mean free time deviates from the Boltzmann mean free time by a factor two. In appendix A the joint distribution of the first and the second free time is calculated for the two-dimensional case. Here too, the distribution of the second free time is not exponential and the average second free time deviates from the Boltzmann value.

In a previous paper[2.4] it has been derived that there is a simple connection between the distribution of the first free time and that of the free times in general. However, this requires a special way of taking averages over different configurations. It is unfeasable to determine the free-time distribution by calculating the third-, fourth-, etc. free-time distribution and taking the average, in view of the complexity of the second-free-time distribution. Below a weighted distribution function of free times will be derived having exact correspondence with the (exponent-ial) distribution of first free times.

Let $M_T(t;x,R^N)\,dt$ be defined as the number of free times between t and $t + dt$ when the moving particle is followed for a time T, starting at x in a configuration of scatterers R^N. Since each of the free times larger than t on the trajectory contains one first free time of value t, one has the equality

$$\int_t^\infty M_T(t'';x,R^N)\,dt'' = \int_0^T \delta(t_1\{x(t'),R^N\} - t)\,dt' \ .$$
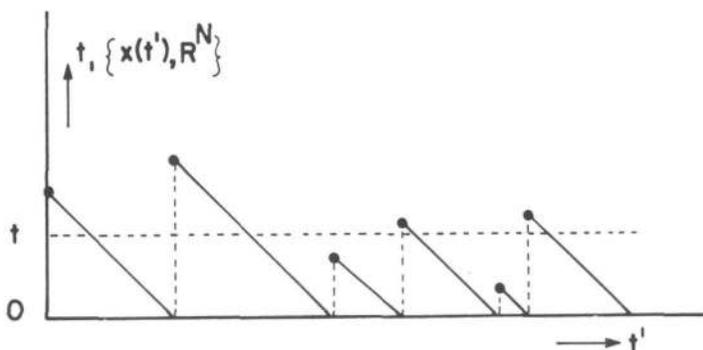
(2.56)

Fig. 2.4. *The first free time t_1 as a function of the trajectory time t'.*
The discontinuities are caused by collisions. Each dot repre-
sents a free time. Each free time larger than t contains one
first free time equal to t.

This is illustrated in fig. 2.4, where it should be noted that each value
$x(t')$, on the trajectory, is a valid starting point for a first free time.
The integration from 0 to T on the right-hand side is enclosed in
$M_T(t'';x,R^N)$ by definition. Furthermore $x(t')$ is a dynamical variable,
$x = (\vec{p},\vec{q})$, with the momentum $\vec{p}$ changing discontinuously due to collisions
and $\vec{q}$ changing continuously with time because of free streaming.

We want to make use of ergodicity but care must be taken because of
the occurrence of pockets. Let a pocket in a configuration R^N be defined
as a region which is enclosed on all sides by scatterers (in the picture
that the scatterers are overlapping particles of radius σ and the moving
particle is a point-particle). In a configuration R^N without pockets,
ensemble and time averages are equal:

$$<\delta(t_1\{x,R^N\} - t)>_x = \lim_{T\to\infty} \frac{1}{T} \int_0^T \delta(t_1\{x(t'),R^N\} - t)\, dt' \quad , \qquad (2.57)$$

where $<...>_x$ denotes the average over all possible x, keeping $|\vec{p}|$ fixed.
In a configuration with pockets this equality holds for each pocket
separately. The average over all configurations R^N, to be taken below,
has to be extended by an average over all pockets in that case. Since

this aspect merely complicates the notation, it will not be taken into account in the following.

Corresponding to $P_N(t)$ a distribution function of first free times for one configuration can be defined: $P(t;R^N)$. From an equation similar to (2.47),

$$P(t;R^N) = <\delta(t_1\{x,R^N\} - t)>_x \quad , \tag{2.58}$$

one finds with (2.56) and (2.57)

$$P(t;R^N) = \lim_{T\to\infty} \frac{1}{T} \int_t^\infty M_T(t";x,R^N)dt" \quad . \tag{2.59}$$

In the computer experiment a histogram is obtained which gives the relative frequency $m_T(t_k;x,R^N)$ in interval k:

$$m_T(t_k;x,R^N) = [N_T(x,R^N)(t_k-t_{k-1})]^{-1}\int_{t_{k-1}}^{t_k} M_T(t";x,R^N)dt" \quad . \tag{2.60}$$

Here $N_T(x,R^N)$ is the number of collisions occurring on the trajectory and the result is made independent of the width of the interval, (t_k-t_{k-1}), by dividing by the width. The mean free time $\tau_T(x,R^N)$ of a trajectory in a configuration R^N, the moving particle being followed for a time T starting at x, is defined by the relation

$$\tau_T(x,R^N) = T/N_T(x,R^N) \quad . \tag{2.61}$$

Elimination of $M_T(t";x,R^N)$ from (2.59) and (2.60) gives

$$\lim_{T\to\infty} m_T(t_k;x,R^N)/\tau_T(x,R^N) = [P(t_{k-1};R^N) - P_t(t_k;R^N)]/(t_k-t_{k-1}). \tag{2.62}$$

The average over all possible configurations is

$$\lim_{T\to\infty} m_T(t_k;x,R^N)/\tau_T(x,R^N)>_R N = [P_N(t_{k-1}) - P_N(t_k)]/(t_k-t_{k-1}). \tag{2.63}$$

It should be noted that pockets can be taken into account by including

an average over x on the left-hand side. An explicit expression for the right-hand side follows from substitution of (2.53) or, in the limit $N \to \infty$, of (2.54). Thus the experimental (measurable) left-hand side of eq. (2.63) should be equal to the theoretical right-hand side (2.63).

Some additional remarks should be made regarding the mean free time. For the derivation of (2.13) the expression for the collision rate Γ was inverted to give the Boltzmann mean free time. Because the scatterers are point-particles, this was originally believed to be the correct mean free time. As will be shown in chapter 4 the experimental mean free time shows significant deviations from this expression at high densities. It was point-ed out by Wood[2.5], that the problem arises because averaging and inversion are non-commuting operations and for higher densities this apparently demonstrates itself. So one cannot expect in general that the average, over different configurations, of the mean free time per configuration (inverse collision rate) is equal to the mean free time calculated by inverting the average collision rate. More explicitly, one can write for the first average τ_e:

$$\tau_e = N_c^{-1} \sum_{\alpha=1}^{N_c} T/N_T(\alpha) = T \, N_c^{-1} \sum_{\alpha=1}^{N_c} N_T^{-1}(\alpha) \quad , \tag{2.64}$$

denoting different configurations (x, R^N) by α and averaging over N_c configurations. The correct average τ_e' is given by

$$\tau_e' = N_c^{-1} \sum_{\alpha=1}^{N_c} T \; / \; N_c^{-1} \sum_{\alpha=1}^{N_c} N_T(\alpha) = T \; / \; N_c^{-1} \sum_{\alpha=1}^{N_c} N_T(\alpha) \quad . \tag{2.65}$$

The same problem is met in averaging the distribution of free times. Analogous to (2.64) a straightforward average, $q_e(s_k)$, over configurations can be defined in terms of the normalized distribution per configuration $m_T(s_k; \alpha)$:

$$q_e(s_k) \equiv N_c^{-1} \sum_{\alpha=1}^{N_c} m_T(s_k; \alpha) \quad . \tag{2.66}$$

Analogous to (2.65) an alternative average $q_e'(s_k)$ can be defined

$$q'_e(s_k) \equiv \sum_{\alpha=1}^{N_C} m_T(s_k;\alpha) N_T(\alpha) / \sum_{\alpha=1}^{N_C} N_T(\alpha) =$$

$$= (\tau'_e/T) \, N_C^{-1} \sum_{\alpha=1}^{N_C} m_T(s_k;\alpha) \, N_T(\alpha) \quad . \tag{2.67}$$

It is easily verified that the alternative average over the distributions is in correspondence with the left-hand side of (2.63) and only differs from it by a factor τ'_e.

It is worth mentioning here how the alternative average affects the results for the one-dimensional system. In the first place it yields the correct Boltzmann value for the mean free time. Secondly it gives a pure exponential behaviour for the free-time distribution.

2.4. Finite-size effects

One of the main concerns in computer experiments simulating infinite systems is always the size of the system, which is here determined by the number of scatterers N. The N-dependence can rarely be analysed rigorously and practically always it has to be done experimentally. The results of such an analysis will be discussed in section 4.3. Yet, it would be very convenient to have beforehand an estimate of the N-dependence as a function of the density.

The clearest defect a small system can show is that the moving-particle passes through the system without undergoing collisions. By the application of periodic boundary conditions this will partially be remedied, but not completely because in some cases the moving particle may continue to walk through the system without collisions (channelling). So the number of free times larger than the time t_L^*, needed by the moving particle to travel across the system, should be kept small.

Let us assume that the free-time distribution is identical to the distribution of first free times, eq. (2.54), which is a reasonable approximation for long times as follows from the appendix and the experimental results. Then, the fraction f of the free times larger than

$t_L^* \, (=L^* = \Omega^{1/d} /\sigma)$ can be computed. This gives for two and three dimensions respectively:

$$f = \exp - t_L^*/\tau^* = \begin{cases} \exp - 2(Nn^*)^{\frac{1}{2}} & \text{for } d = 2 \\ \\ \exp - \pi N^{\frac{1}{3}} n^{*\frac{2}{3}} & \text{for } d = 3 \end{cases} \quad .(2.68)$$

So one needs larger N for smaller densities to keep f below a certain value. Some of the highest values for f are for the two-dimensional systems studied: $f = 1.8 \times 10^{-3}$ for N = 2000 and $n^* = 0.005$, $f = 7.2 \times 10^{-7}$ for N = 500 and $n^* = 0.1$. For the three-dimensional case one has: $f = 0.14$ for N = 100 and $n^* = 0.05$, $f = 0.16$ for N = 2000 and $n^* = 0.01$.

In the three-dimensional case the given values of f are rather high, but not all the free times contained in f lead to erroneous contributions. One special event that does give errors consists of successive collisions of the moving particle with a scatterer and one of its nearest images across the periodic boundary. For this situation a geometrical factor can be calculated, determined by the angles under which a scatterer sees its periodic images. Multiplication of f with this geometrical factor gives the probability that this special event takes place. Assuming a random orientation of the velocity after the first collision, one finds for the geometrical factor f_g in the two-dimensional case: $f_g = 2 \times 10^{-3}$ for N = 2000, $n^* = 0.005$ and $f_g = 2 \times 10^{-2}$ for N = 500, $n^* = 0.1$. The product of f and f_g gives an extremely small probability for this special event in both situations. In three dimensions one finds for the geometrical factor: $f_g = 1 \times 10^{-2}$ for N = 100, $n^* = 0.05$ and $f_g = 4 \times 10^{-4}$ for N = 2000, $n^* = 0.01$.

Other events like travelling repeatedly across the system without collisions are not so easily handled. The results in section 4.3 indicate that their influence is dominant. However, the most important result of this section is that once it has been established that within a given accuracy a system is large enough for a certain density, it will be the more so for higher densities.

References

2.1) Van Leeuwen, J.M.J. and Weyland, A., Physica $\underline{36}$ (1967) 457

2.2) Weyland, A. and van Leeuwen, J.M.J., Physics $\underline{38}$ (1968) 35

2.3) Ernst, M.H. and Weyland, A., Phys. Letters $\underline{34A}$ (1971) 39

2.4) Bruin, C., Physica $\underline{72}$ (1974) 261

2.5) Wood, W.W., private communication

3. METHOD OF COMPUTATION

3.1. Monte Carlo method

In the computer experiment one has to simulate for a given density n^* an infinite system of point-scatterers with one moving particle of radius σ. The trajectory of the moving particle has to be computed, starting from a given position with given velocity, and the average over all possible initial conditions of the moving particle has to be performed. This has been approximated by generating many different configurations of a finite number of scatterers N and by computing the trajectory of the moving particle in each configuration for one initial condition. The number N should be large enough to make finite-size effects sufficiently small.

Since the scatterers are point-particles, the configurations can be obtained from a crude Monte Carlo method: the coordinates should be chosen from random numbers uniformly distributed on the interval $(0, L^*)$. This holds only partly for the coordinates of the moving particle since they should not give overlap with one of the scatterers.

The (pseudo-)random number generator used is RANDU from IBM[3.1]. This is a multiplicative congruential generator, so it generates a random integer U_{i+1} from U_i according to

$$U_{i+1} = a.U_i \text{ modulo } M ,\qquad\qquad (3.1)$$

where one has for the multiplier $a = 65539 = 2^{16} + 3$ and for the modulus $M = 2^{31}$, the exponent being equal to the word size of the machine minus one sign-bit.

Many tests on the randomness of numbers produced by random generators have been developed, see e.g. Knuth[3.2]. Multiplicative congruential

generators for which a is of the order of $\sqrt{M}$ pass quite a number of tests[3.3]. The tests on uniformity and serial correlation have been performed by the author on the generator used here (3.1), showing random behaviour with high accuracy. However, congruential generators do show serious deviations from randomness with respect to d-tuples, being important for the case that consecutive (pseudo-) random numbers are used as coordinates in d-dimensional space. This has been found by MacLaren and Marsaglia[3.3] for triples (d = 3) and this feature has been explained by Marsaglia[3.4] by showing that 'random numbers fall mainly in plains'. The upper bound for the number of plains containing all d-tuples appears to decrease rapidly with d. Some tests sensitive in this respect are the r^2 test[3.5] and the test on d-dimensional uniformity. In the r^2 test one computes the distribution of distances r occurring in a d-dimensional cube between points having (pseudo-) random numbers as coordinates. In a test on d-dimensional uniformity the d-dimensional cube is divided in smaller cubes (cells) and the occupation numbers of the cells are computed.

The distribution of free times and the mean free time, obtained from the trajectory of a moving particle in a configuration of scatterers can also provide a check on the randomness of a configuration. Though there are some problems in the theoretical expressions for these quantities (section 2.3), they turned out to be useful.

For the 2-dimensional configurations the coordinates of the scatterers (x_i, y_i) have been obtained from the generator (3.1) consecutively:

$$x_i = U_{2i-1} \ L^*/M \ , \quad y_i = U_{2i} \ L^*/M \ . \tag{3.2}$$

Although this way of generation suffers from the above-mentioned defect, the number of planes containing all the positions appears to be sufficiently large to let the generator pass all three tests, even if the width of the interval in the r^2 test or the cell-size in the 2-dimensional uniformity test is made small (of the order of $L^*/100$ to $L^*/ 1000$).

For the 3-dimensional configurations the strategy of eq (3.2)

$$x_i = U_{3i-2} \ L^*/M, \quad y_i = U_{3i-1} \ L^*/M, \quad z_i = U_{3i} \ L^*/M, \tag{3.3}$$

leads to configurations failing all three tests, thus being significantly non-random. Another way of obtaining the coordinates from the same generator,

$$x_i = U_i \ L^*/M, \quad y_i = U_{N+i} \ L^*/M, \quad z_i = U_{2N+i} \ L^*/M, \tag{3.4}$$

turned out to give satisfactory results for all three tests. Therefore eq. (3.4) has been used for the generation of 3-dimensional configurations, see also R. Amadori[3.6].

3.2. Molecular-dynamics method.

The subject of this section is the solution of the equation of motion of the moving particle in a given configuration of scatterers. In addition to the generation of positions (section 3.1) the initial velocity of the moving particle and the boundary conditions have to be specified. As usual in this type of computations periodic boundary conditions are imposed on the system. In this case they result in a model of one particle moving in an infinite lattice with the chosen configuration of scatterers as unit cell. The magnitude of the velocity is a constant of motion and is used as a scaling quantity. The initial direction is chosen at random.

It follows from the hard-sphere interaction, eq. (2.2), that the moving particle undergoes instantaneous collisions, changing its velocity in direction, and that it moves freely between the collisions. The algorithm for this type of motion is a simplification of the one already described by Alder and Wainwright[3.7]. The relation between the velocities before and after a collision, $\vec{v}$ and $\vec{v}'$ respectively, reads

$$\vec{v}' = \vec{v} - 2 \ (\vec{v} \cdot \vec{\sigma}_i) \vec{\sigma}_i / \sigma^2 , \tag{3.5}$$

where one has $\vec{\sigma}_i = \vec{q} - \vec{R}_i$, $\vec{q}$ denoting the position of the moving particle

at the moment it collides with scatterer i at position $\vec{R}_i$. For the determination of the moment t_i of the collision between the moving particle starting from $\vec{q}(0)$ and scatterer i at $\vec{R}_i$, assuming that the other scatterers do not interfere, one uses the equation

$$\vec{q}(0) + \vec{v}t_i - \vec{R}_i = \vec{\sigma}_i \ . \tag{3.6}$$

The solution for the time t_i from this equation, which can be obtained after taking the square, reads

$$t_i = - \vec{v}.(\vec{q}(0)-\vec{R}_i)/v^2 \pm [\{\vec{v}.(\vec{q}(0)-\vec{R}_i)/v^2\}^2 - \{(\vec{q}(0)-\vec{R}_i)^2-\sigma^2\}/v^2]^{\frac{1}{2}}.$$
$$\tag{3.7}$$

This may result in (see fig. 3.1):

1) no real roots (no collision),

2) negative roots (collision in the past),

3) one or two positive roots (the smallest root is the physical one).
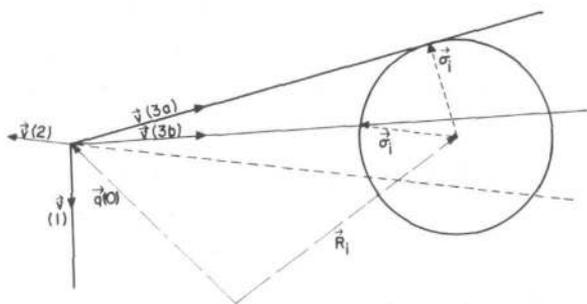
Fig. 3.1. *Solutions of eq. (3.6). The indices correspond to the cases mentioned below eq. (3.7).*

Starting from an initial state $(\vec{q}(0),\vec{v})$ the smallest positive t_i (i = 1, 2,..., N) determines the next collision. The particle freely moves for a time t_i, the change in direction of the velocity due to the collision is computed and the procedure is repeated. The computation of t_i for all scatterers before every collision demands a lot of machine-time.

However, the computing time can be reduced by considering only the scatterers in the neighbourhood of the moving particle. For this purpose a grid is imposed on the system, with a cell size that is considerably smaller than the volume of the system. This of course raises the problem that the moving particle could miss a collision with a scatterer lying in an adjacent cell.

One way to overcome this problem is to enlarge the cells by a region of width σ in all the coordinate-directions, thus giving the cells an overlapping region of width 2σ. These enlarged cells can now be treated separately. A dummy free time is introduced which represents the time it takes for the moving particle to reach the boundary of its cell. If the moving particle does not collide with one of the scatterers of its cell before it crosses the boundary at some position, that position is taken as a new starting point and the procedure is repeated in the adjacent cell. In enlarging the cells the periodic boundary conditions have to be taken into account. During the motion these conditions can easily be handled by computing the number of the adjacent cell properly. This method has been used for the computations in two dimensions.

For the 3-dimensional case this method was too extensive to program and therefore another method was chosen which is equally efficient. In that method there is no overlap between the cells. The problem of missing a collision is solved by considering all surrounding cells (there are 26 of them, in three dimensions) together with the cell in which the moving particle is. In this cube of 27 cells a cube is defined smaller by an amount of σ in all coordinate-directions. The smallest free time found within this smaller cube determines the next collision. After performing the collision the whole procedure is repeated, if necessary in an adjacent cell. If the computed next collision would have to take place outside the smaller cube, there is no guarantee that it is indeed the next one. The particle is moved to the boundary of the adjacent cell and the whole procedure is repeated. If no collision is found with any of the scatterers within the 27 cells, the particle is moved to the boundary of its cell and only a limited number of cells (9) have to be considered in the following step. To facilitate the handling of the periodic boundary conditions in

this case, the system is enlarged with a layer of a thickness of one cell in all coordinate-directions.

In both methods the optimal number of cells depends upon the number of scatterers and also the density. In the first method the lower bound on the number of cells is trivial, being 1, and the minimum length of a cell is 2σ. In the second method the lower bound on the number of cells is 27 and the minimum length of a cell is σ.

3.3. Correlation functions

The numerical solution of the equation of motion results in the velocity $\vec{v}(s)$ and the position $\vec{q}(s)$ of the moving particle as a function of the reduced time $s = t/\tau$, measured with respect to the initial state of the moving particle. The correlation functions at a certain density are obtained as an average over N_f correlation sequences for one configuration of scatterers and an average over the results of N_c configurations. The normalized velocity autocorrelation function of the moving particle is

$$\phi(s_\ell) = \frac{1}{N_c N_f} \sum_{j=1}^{N_c} \sum_{i=1}^{N_f} \vec{v}(s_i) \cdot \vec{v}(s_i + s_\ell)/v^2 , \qquad (3.8)$$

where the dependence of $\vec{v}$ on configuration j is not indicated explicitly. Similarly the mean square displacement is obtained as

$$\Delta(s_\ell) = \frac{1}{N_c N_f} \sum_{j=1}^{N_c} \sum_{i=1}^{N_f} (\vec{q}(s_i + s_\ell) - \vec{q}(s_i))^2/\sigma^2 . \qquad (3.9)$$

The integer ℓ runs from zero to a maximum value ℓ_{max} and one has $s_\ell = h\ell$, h being the time increment with which the correlation function is sampled. The starting time of correlation sequence i is s_i on the absolute time scale.

It saves computing time for the solution of the equation of motion if the delay $s_i - s_{i-1}$ between two succeeding correlation sequences,

i - 1 and i, is taken much smaller than the maximum time $h\ell_{max}$ for which
the correlation sequence is sampled. On the other hand if one would take
the delay as small as the time increment h, the information is still so
much correlated that succeeding correlation sequences scarcely improve the
statistical accuracy. The time-delay s_i-s_{i-1} is thus to be chosen as a com-
promise between minimizing the total time the moving particle is followed
in a configuration and minimizing the number of correlation sequences needed
to obtain a certain statistical accuracy. The value $s_i-s_{i-1} = \frac{1}{2}$, measured
in units of τ, has been adopted in many cases; other values being $\frac{3}{4}$ and 1.

In the machine program, the values of a number of correlation sequences
at their respective s_ℓ are computed at a certain time s, where ℓ follows
from $\ell = s_\ell/h = (s - s_i)/h$ for each sequence i. One is only interested in
values of ℓ which satisfy the condition $0 < \ell < \ell_{max}$. This condition de-
termines the correlation sequences which are to be considered at time s.
For each sequence the starting conditions $\vec{q}(s_i)$ and $\vec{v}(s_i)$ are still
kept in memory at s. In this way of programming it saves time to have the
time-delay s_i-s_{i-1} as a multiple of h.

Another way of computing correlation functions can be found from the
observation that the average over i in eq. (3.8) is a discrete convolution,
as was pointed out by Futrelle and McGinty[3.8]. By taking discrete fourier
transforms the number of operations can be reduced considerably, especially
when the fast-fourier-transform (FFT) technique is used. However, for the
low-density calculations that are our main objective, this method turned
out to take more machine-time on comparison. The reason for this can
easily be understood from the observation that the time-delay between two
succeeding functions in the FFT method is inherently equal to the time
increment h. So this method samples less efficiently than the method
described before. Moreover there is the disadvantage that the statistical
accuracy of the correlation function decreases for longer times. The
situation is even worse in the case of high densities where the velocity
autocorrelation function has a long negative tail. In the method used
here it is possible to work with different time increments at the same
time, a small one for the region where the function decays fast and a
large one to sample the tail which varies slowly. An efficient choice
for the long-time increment is the delay time, s_i-s_{i-1}.

3.4. Diffusion coefficients

The numerical integration of the velocity autocorrelation function
(eq. (2.14)) to obtain the 'experimental' diffusion coefficient is
restricted in its accuracy because of the time increment h adopted and
because of the finite time $h\ell_{max}$ for which the correlation function is
considered. The first point could be settled satisfactorily by taking
h = 0.1 or h = 0.15. Then the error due to the size of h is smaller than
the statistical error. In many cases, when the statistical error was not
extremely small, h = 0.2 could be taken as well. The error due to the
size of h could be estimated by using different integration rules, or
alternatively by applying one integration rule for a number of values
for h and extrapolating these results to h = 0. All results to be men-
tioned later have been obtained with Simpson's integration rule. The
second point cannot be settled so easily, because the required value of
ℓ_{max} depends upon the density and hence cannot be given in general.

The numerical differentiation of the mean square displacement has
been replaced by a least-squares fit of a straight line, the slope of
which is proportional to the diffusion coefficient (eq. (2.15)). The
time increment for the mean square displacement should not be chosen too
small since succeeding points would then be highly correlated. Values
that have been used are h = 0.5 and h = 1. Another important value is
ℓ_{max}, the choice of which is closely related to the problem for the
velocity autocorrelation function: strictly speaking, the mean square
displacement is only a straight line after the velocity autocorrelation
function has become zero. By omitting more and more points of the mean
square displacement in the least-squares fit beginning at small times, one
can find a value of s_ℓ beyond which the slope does not vary outside the
statistical accuracy. This value of s_ℓ has to coincide with the time above
which the velocity autocorrelation function is zero within the limits of
accuracy. So one has two different, though not independent, criteria for
the determination of ℓ_{max}.

3.5. Mean free time and distribution of free times

Most of the experimental mean free times have been computed with
(2.64) and the standard deviations have been obtained from the differences
with the mean value. In a few test runs the validity of the alternative
average (2.65) has been checked. Both types of results have been compared
with the Boltzmann mean free time.

Also most of the average distributions of free times have been ob-
tained using the straightforward average (2.66), which reads more ex-
plicitly

$$q_e(s_k) = N_C^{-1} \sum_{\alpha=1}^{N_C} N_T^{-1}(\alpha) \sum_{\ell=1}^{N_T(\alpha)} \{ H(s_\ell - s_{k-1}) - H(s_\ell - s_k) \}/h , \qquad (3.10)$$

where s_ℓ is the reduced free time (t_ℓ/τ) before the ℓth collision. H de-
notes the Heaviside function, $H(s) = 0$ for $s < 0$ and $H(s) = 1$ for $s \geqslant 0$,
k runs from 1 to a maximum value k_{max} and the time interval of the histo-
gram is $h = s_k - s_{k-1}$. The value $h = 0.05$, almost always used, is small
enough for a detailed sampling of the distribution and is large enough
with respect to statistics. The value $k_{max} = 400$ was almost always large
enough to cover the range of the computed free times. The alternative
average (2.67) has been considered as well in some cases, reading

$$q_e'(s_k) = (\tau_e'/T) N_C^{-1} \sum_{\alpha=1}^{N_C} \sum_{\ell=1}^{N_T(\alpha)} \{ H(s_\ell - s_{k-1}) - H(s_\ell - s_k) \}/h . \qquad (3.11)$$

One way to analyze the obtained histograms is to compare them with
the right-hand side of (2.63), which we denote by $Q_N(s_k)$ and which reads
explicitly

$$Q_N(s_k) = \{ (1 - s_{k-1}\tau/\tau_N N)^{N-1} - (1 - s_k\tau/\tau_N N)^{N-1} \}\tau/\tau_N h . \qquad (3.12)$$

This gives in the thermodynamic limit, $N \to \infty$,

$$Q(s_k) = \exp(-s_k) \{\exp(h) - 1\}/h \ . \tag{3.13}$$

Another way of studying the distribution of free times is to introduce an adjustable parameter η, the inverse of the mean free time, in $Q_N(s_k)$ or $Q(s_k)$ which can take into account that the mean free time deviates from τ_N or τ. The functions

$$Q_N(s_k;\eta) = \eta\{ (1 - \eta s_{k-1}/N)^{N-1} - (1 - \eta s_k/N)^{N-1}\}/h \tag{3.14}$$

and, in the limit $N \to \infty$,

$$Q(s_k;\eta) = \eta \exp(-\eta s_k) \{\exp(\eta h) - 1\}/h \tag{3.15}$$

are obvious generalizations of (3.12) and (3.13) respectively.
As mentioned at the end of section 2.3 $q_e'(s_k)$ differs from the left-hand side of eq. (2.63) by a factor τ_e'. This difference can be easily accounted for by absorbing this factor in (3.14) or (3.15), giving after cancellation against the factor η the functions

$$\hat{Q}_N(s_k;\eta) = \{ (1 - \eta s_{k-1}/N)^{N-1} - (1 - \eta s_k/N)^{N-1}\}/h \tag{3.16}$$

and

$$\hat{Q}(s_k;\eta) = \exp(-\eta s_k)\{ \exp(\eta h) - 1\}/h \ . \tag{3.17}$$

These same functions $\hat{Q}_N(s_k;\eta)$ and $\hat{Q}(s_k;\eta)$ have been used for the analysis of $q_e(s_k)$. Although the choice between (3.14), (3.15) and (3.16), (3.17) is less unique in this case, we have decided to do so, because $q_e(s_k)$ and $q_e'(s_k)$ have the same dimensionality. The results justify this choice. A least-squares fit of $\hat{Q}_N(s_k;\eta)$ or $\hat{Q}(s_k;\eta)$ provides us with a value for η_e, which is an estimate for the inverse mean free time.

References

3.1) System/360 Scientific Subroutine Package
    IBM Application Program GH20 - 0205 - 4

3.2) Knuth, D.E., The art of computer programming Vol. 2.
    Addison-Wesley Publishing Company, Reading (MA) (1969)

3.3) MacLaren, M.D. and Marsaglia, G., J.A.C.M. 12 (1965) 83

3.4) Marsaglia, G., Proc. Nat. Acad. Sci. 61 (1968) 25

3.5) Gruenberger, F. and Mark, A.M., Math. Tables Other Aids Comp. 5
    (1951) 109

3.6) Amadori, R., J. Comp. Phys. 24 (1977) 450

3.7) Alder, B.J. and Wainwright, T.E., J. Chem. Phys. 31 (1959) 459

3.8) Futrelle, R.P. and McGinty, D.J., Chem. Phys. Letters 12 (1971)
    285

4. COMPUTATIONAL RESULTS

4.1. Two-dimensional Lorentz gas

The computations for the two-dimensional Lorentz gas have been per-
formed from very low densities, where deviations from the Boltzmann regime
are small, up to high densities, where diffusion becomes impossible. As
has been shown in chapter 2, the effect of finite N, the number of scat-
terers, is larger for lower densities. Therefore, in general the values of
N used for low densities have been chosen larger than those for the higher
densities. Since the verification of a series expansion in the density is
the main object, the major part of machine time has been spent on the low-
density region.

In table 4.1 the characteristic parameters and most important results
of the molecular-dynamics computations are given. The various columns
contain respectively

1) the reduced density n^*,
2) the number of scatterers N,
3) the number of configurations of scatterers N_c,
4) the total number of correlation sequences $N_f N_c$ used in the
   averaging procedure,
5) the experimental mean free time τ_e reduced with respect to the
   Boltzmann infinite-system mean free time τ,
6) the reciprocal of the collision rate η_e as obtained from a
   least-squares fit of the distribution of free times,
7) the normalized χ^2-variable resulting from the above-mentioned fit,
8) the reduced diffusion coefficient $D_e/v\sigma$, as obtained from inte-
   grating the velocity autocorrelation function. Up to the density
   $n^* = 0.1$ this function has been computed in 100 equidistant points.

Table 4.1. Characteristic parameters and results[a] for the 2-dimensional Lorentz gas.

1	2	3	4	5	6	7	8	9	10	11
n^*	N	N_c	$N_f N_c$ (10^6)	τ_e/τ	η_e^{-1}	χ^2	$D_e/v\sigma$	s_x	$D_e/v\sigma$	s_n, s_x
0.003	8000	800	20	0.9995(3)	0.9994(3)	1.07	61.20(9)	15		
0.004	8000	800	20	0.9993(3)	0.9990(3)	1.15	45.69(6)	15		
0.004	8000	4000	10	0.9999(3)	0.9997(4)	1.15	45.68(10)	15		
0.005	8000	800	20	0.9995(3)	0.9992(3)	1.23	36.34(5)	15		
0.005	2000	3200	40	1.0004(3)	1.0002(3)	1.24	36.40(4)	10		
0.010	8000	1600	20	0.9997(3)	0.9994(3)	1.17	17.80(2)	15		
0.010	2000	1600	20	0.9999(4)	0.9999(3)	0.95	17.77(3)	10		
0.015	8000	800	10	0.9995(4)	0.9991(4)	1.19	11.59(2)	15		
0.015	2000	1600	20	1.0001(4)	1.0000(3)	0.95	11.57(2)	10		
0.020	8000	1600	20	0.9995(4)	0.9992(3)	1.01	8.525(13)	15		
0.020	2000	1600	20	1.0002(4)	1.0000(3)	1.07	8.547(13)	10		
0.030	2000	400	5	1.0003(5)	0.9998(6)	1.02	5.498(16)	15		
0.040	2000	400	5	0.9983(7)	0.9975(5)	0.92	3.931(11)	15		
0.050	2000	280	3.5	1.0005(11)	0.9998(7)	1.27	3.049(10)	15		
0.050	2000	2000	1	1.0018(12)	1.0003(10)	1.09	3.039(16)	20	3.014(28)	20,100
0.050	alternative			0.9985(11)	0.9973(10)	1.05				
0.060	2000	400	2	0.999(1)	0.998(1)	1.02	2.424(13)	20		
0.070	2000	320	1.6	0.999(1)	0.998(1)	1.15	2.033(12)	20		
0.080	2000	240	1.2	0.998(2)	0.998(1)	0.97	1.692(10)	20		
0.090	2000	160	0.8	0.997(2)	0.995(1)	0.98	1.442(11)	20		
0.100	2000	160	0.8	0.998(2)	0.996(1)	1.01	1.255(11)	20		

Table 4.1. (continued).

1 n^*	2 N	3 N_c	4 $N_f N_c$ (10^6)	5 τ_e/τ	6 η_e^{-1}	7 χ^2	8 $D_e/v\sigma$	9 s_x	10 $D_e/v\sigma$	11 s_n, s_x
0.10	500	200	0.5	0.999(3)	0.994(2)	1.23	1.217(22)	30	1.207(21)	30,50
0.12	500	200	0.5	1.004(4)	1.000(2)	1.08	0.934(20)	30	0.918(28)	30,50
0.14	500	200	0.5	1.002(4)	0.994(2)	1.23	0.717(14)	30	0.702(16)	30,50
0.16	500	200	0.5	1.002(7)	0.996(2)	1.09	0.600(11)	30	0.610(12)	30,50
0.18	500	200	0.5	1.007(7)	0.997(3)	1.42	0.458(7)	30	0.462(12)	30,50
0.20	2000	2000	1	1.021(3)	1.016(1)	1.67	0.385(8)	30	0.368(5)	30,100
0.20	alternative			0.994(6)	0.995(1)	1.02				
0.20	500	200	0.5	1.014(5)	1.002(3)	2.04	0.364(8)	30	0.365(9)	30,50
0.22	500	200	0.5	1.014(11)	1.003(3)	1.21	0.308(8)	45	0.304(8)	45,50
0.24	500	200	0.5	1.025(8)	1.014(3)	1.66	0.249(6)	45	0.248(6)	45,50
0.26	500	200	0.5	1.029(10)	1.018(3)	1.22	0.206(6)	45	0.207(7)	45,50
0.28	500	200	0.5	1.055(12)	1.036(3)	1.73	0.153(3)	45	0.156(5)	45,50
0.30	500	200	0.5	1.066(9)	1.046(4)	2.82	0.139(5)	45	0.137(5)	45,50
0.40	2000	2000	1	1.115(5)	1.089(4)	11	0.037(3)	90	0.040(2)	90,100
0.40	alternative			1.018(9)	1.005(2)	1.64				
0.60	2000	2000	1	1.190(9)	1.148(5)	16				
0.60	alternative			1.000(10)	0.989(2)	1.41				
0.80	2000	2000	1	1.283(13)	1.211(6)	21				
0.80	alternative			1.011(17)	1.004(2)	1.17				

[a]Notation: 0.9995(3) = 0.9995 ± 0.0003; 1.283(13) = 1.283 ± 0.013.

Time increments of $h = 0.1$, 0.15 or 0.2 have been used. For den-
sities higher than $n^* = 0.1$, in addition to the 100 points with
$h = 0.1$ or 0.2 the velocity autocorrelation function has been
computed in 80 points with a 5 times larger time increment:
$h = 0.5$ or 1.0,

9) the maximum time s_x up to where the velocity autocorrelation
   function has been integrated,

10) the reduced diffusion coefficient $D_e/v\sigma$, as obtained from the
    slope of the mean square displacement,

11) the minimum time s_n and the maximum time s_x between which the
    slope has been determined.

For the lines marked by the word 'alternative' in the second column,
the same configurations of scatterers and trajectories of the moving
particle have been used as in the preceding line to compute the alternative
averages, τ'_e (2.65) and $q'_e(s_k)$ (3.11), instead of the straight-forward
averages.

For low densities up to a density $n^* = 0.2$ it is found that τ_e/τ is
in good agreement with the value 1, taking into account the standard
deviation. (Reducing τ_e with respect to τ_N instead of τ gives a negligible
change in the numbers). For higher densities τ_e/τ becomes significantly
too high. For the few cases studied at high density, τ'_e/τ does appear to
be in agreement with the theoretical value 1.

For the case of the Ehrenfest wind-tree model, Wood[4.1] has also
observed that τ_e is a good approximation to τ'_e for low densities and a
bad one for high densities. His explanation for this effect is that for
higher densities the distribution of mean free times, as obtained for
different configurations of scatterers, becomes broader. This leads to
larger values for the higher relative moments of the distribution and
these become non-negligible in an expansion of τ_e in terms of τ'_e. More
explicitly, one can make an expansion of the average of the inverse of
variable t in terms of the inverse of the average of t and one obtains

$$\langle t^{-1} \rangle = \langle t \rangle^{-1} \langle \{1 + \frac{t - \langle t \rangle}{\langle t \rangle}\}^{-1} \rangle$$

$$= \langle t \rangle^{-1} \{1 + \frac{\langle \{t - \langle t \rangle\}^2 \rangle}{\langle t \rangle^2} - \frac{\langle \{t - \langle t \rangle\}^3 \rangle}{\langle t \rangle^3} + \ldots\} . \qquad (4.1)$$

The fitted values η_e for η have been obtained from a minimization procedure for the reduced χ^2-variable

$$\chi^2 = (1/199) \, \Sigma_{k=1}^{200} \, \{\hat{Q}(s_k; \eta) - q_e(s_k)\}^2 / \sigma_k^2 , \qquad (4.2)$$

where $\hat{Q}(s_k; \eta)$ and $q_e(s_k)$ are defined in (3.16) and (3.9) respectively and σ_k is the standard deviation of $q_e(s_k)$. Only the first 200 intervals of the distributions have been used rather than all the 400 computed ones because of the smaller statistical accuracy of the last 200 intervals. The standard deviations of η_e have been obtained from the variance-covariance matrix in the fitting procedure.

The inverted values η_e^{-1} behave in much the same way as τ_e/τ. Of course, for the so-called alternative lines in table 4.1 $q_e'(s_k)$, defined in (3.10), has been used in eq. (4.2) rather than $q_e(s_k)$.

The reduced χ^2-variable gives a measure for the correctness of the fit. For the lower densities the values for χ^2 are in reasonable agreement with the most probable value 1, be it that they are somewhat high in general. For high densities the deviations from 1 are significant as regards the results for the straightforward average $q_e(s_k)$. Again for the alternative average $q_e'(s_k)$ the results are quite satisfactorily close to 1. In fig. 4.1 a few examples are given of the behaviour of the terms $\chi_k = \{q_e(s_k) - \hat{Q}(s_k; \eta_e)\}/\sigma_k$ and $\chi_k' = \{q_e'(s_k) - \hat{Q}(s_k; \eta_e)\}/\sigma_k$ occurring in the sum of eq. (4.2). Only the first 120 values of k are shown, giving a range for the reduced time s_k from 0 to 6.

As regards the alternative average χ_k', the major part of the values is situated between + 1 and - 1 as expected. For a low density, $n^* = 0.05$, this also holds for the straightforward average χ_k. For a high density, $n^* = 0.8$, large deviations from the expected behaviour are observed.
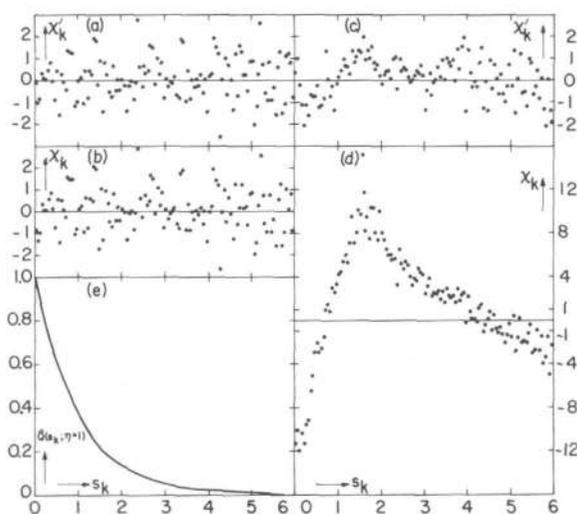
Fig. 4.1. Details of the 2-dimensional free-times distribution. For the low-density case $n^* = 0.05$ ($N = 2000$, $N_c = 2000$) χ'_k is given in (a) and χ_k in (b). For the high-density case $n^* = 0.8$ χ'_k is given in (c) and χ_k in (d). In (e) $\hat{Q}(s_k; \eta = 1)$ is given for reference to an absolute scale. The abscissa is identical in all cases.

Qualitatively these deviations are in agreement with the differences be-tween the free-times distributions of the first and the second free time, shown in fig. A.6.

The diffusion coefficients obtained from the velocity autocorrelation function agree reasonably well with those from the mean square displace-ment, as should be. For further analysis the former ones have been used. In case more than one value is mentioned in column 8 of table 4.1 at the same density, the average has been determined using weight factors pro-portional to the inverse square of the pertinent standard deviations.

In fig. 4.2 the inverted experimental diffusion coefficients are given as a function of the density. Error bars have been omitted when they are smaller that the dots. For low densities (up to $n^* = 0.1$) the agreement with the first few terms of the density expansion (2.25) is very good.
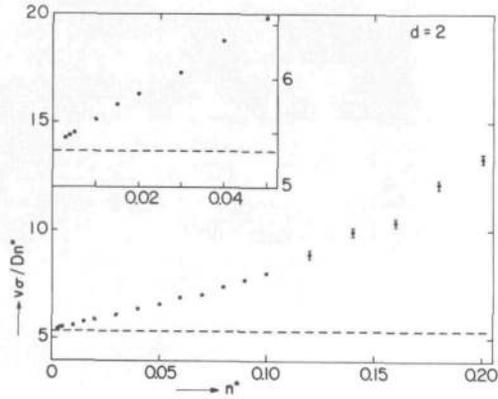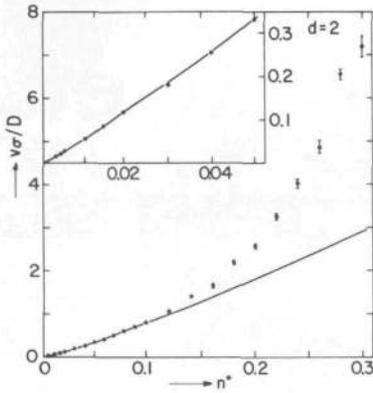
Fig. 4.2. *The experimental inverse diffusion coefficient as a function of the density for the 2-dimensional case (dots). The sum of the first four terms in the density expansion,* $v\sigma/D = c_1 n^* + c_2' n^{*2} \ln n^* + c_2 n^{*2} + c_3'' n^{*3} (\ln n^*)^2$, *is presented by the line. For low densities the data are shown on an enlarged scale.*

Fig. 4.3. *Comparison of* $v\sigma/D_e n^*$ *(dots) with the Boltzmann term* $c_1 = 16/3$ *(dashed line).*

For a closer inspection of the low-density region, $v\sigma/D_e$ is divided by n^* and the result is compared in fig. 4.3 with the Boltzmann value c_1 (dashed line). For decreasing densities, $v\sigma/D_e n^*$ converges rather well towards c_1, which is the leading contribution for low densities.

Next, the Boltzmann contribution c_1 is subtracted from $v\sigma/D_e n^*$ and the difference is again divided by the density. The resulting data show a remarkable increase for $n^* \to 0$ in fig. 4.4. The seven lowest densities for which the most extensive computations have been carried out show clearly the decrease of the first logarithmic term for increasing density. They indicate that the coefficient c_2' is of the right order of magnitude. From these data it can be concluded that the density expansion of the inverted diffusion coefficient for the 2-dimensional Lorentz gas does contain a logarithmic term.

This conclusion is also suggested by a comparison of the least-squares fits of either $\alpha_0 \ln n^* + \alpha_1 + \alpha_2 n^* (\ln n^*)^2$ or $a_0 + a_1 n^* + a_2 n^{*2}$ to the
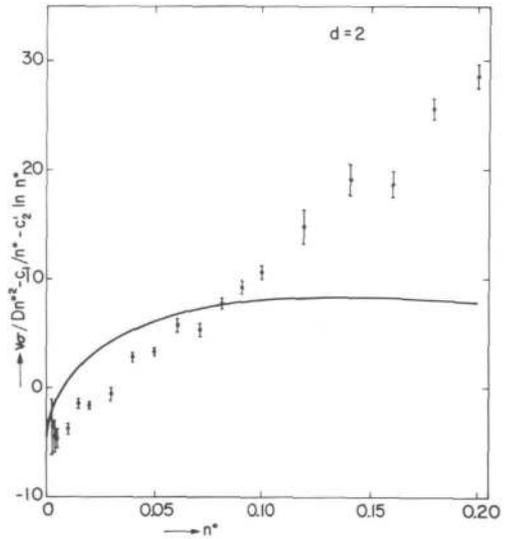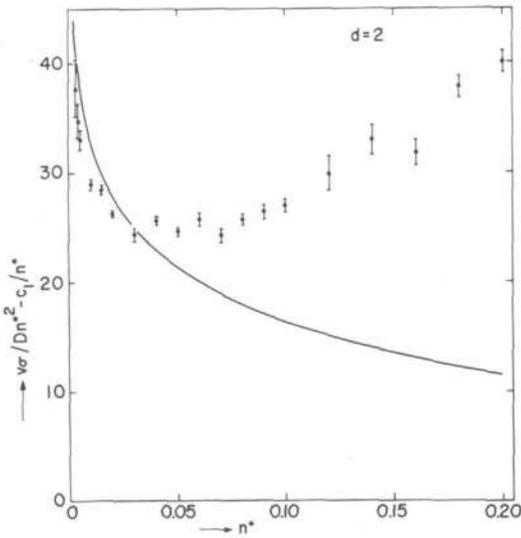
Fig. 4.4. Comparison of $(v\sigma/D_e n^* - c_1)/n^*$ (dots) with the most important logarithmic term $c_2' \ln n^*$ (line).

Fig. 4.5. Comparison of $(v\sigma/D_e n^* - c_1)/n^* - c_2' \ln n^*$ (dots) with the remaining terms $c_2 + c_3'' n^*(\ln n^*)^2$ (line).

experimental data $(v\sigma/D_e - c_1 n^*)/n^{*2}$. This has been done starting from low densities with an increasing number of data points, as given in fig. 4.4. The results for the coefficients are tabulated in table 4.2 for a few cases. Quantitatively, these results are not very meaningful, both because of the large errors for the coefficients and hence their fluctuating values and because of large values for the χ^2- variable, leading to values of about 90% in the χ^2- test (this should be 50%). The important point that this comparison does show is that in case one wants to describe the data with a power series, one needs coefficients increasing by about a factor of 10 with each order.

A more appropriate numerical test on the validity of the series expansion (2.25) is provided by the difference of the experimental inverted diffusion coefficient and the predicted one, divided by the experimental standard deviation: $\chi_{n^*} = (v\sigma/D_e - v\sigma/D)/\sigma_D(v\sigma/D_e)^2$, where

Table 4.2. Least-squares fit results of either $\alpha_o \ln n^* + \alpha_1 + \alpha_2 n^* (\ln n^*)^2$
or $a_o + a_1 n^* + a_2 n^{*2}$ to a number i_{max} of data points as given
in fig. 4.4 starting from low densities. The errors given have
been obtained from the variance-covariance matrix in the fitting
procedure.

i_{max}	α_o	α_1	α_2	a_o	a_1 (10^1)	a_2 (10^2)
6	− 7 (7)	− 9 (44)	21 (6)	37 (2)	−85 (42)	164 (153)
7	− 6 (5)	0.5 (29)	9 (36)	36 (1)	−70 (19)	104 (51)
8	−13 (5)	−44 (30)	67 (36)	36 (3)	−74 (11)	120 (22)
9	−13 (4)	−47 (24)	71 (28)	34 (2)	−53 (12)	68 (20)
10	−14 (4)	−53 (26)	79 (30)	34 (1)	−47 (10)	58 (14)

σ_D is the standard deviation in $D_e/v\sigma$. The absolute value of χ_{n^*} should
be of order 1 and the + and − signs should be distributed at random.
From the second column of table 4.3 it is clear that χ_{n^*} fails the test
for the values of the coefficients given in (2.26), even for low densi-
ties. The values are all negative and their amplitude is much too large.
The deviations for higher densities are not so serious, because they can
be accounted for by higher order terms in the series expansion.

In fig. 4.5 the discrepancy is also illustrated, by plotting
$(v\sigma/D_e - c_1 n^* - c_2' n^{*2} \ln n^*)/n^{*2}$ and comparing it with $c_2 + c_3'' n^* (\ln n^*)^2$.
From this figure one might prefer a larger negative value for c_2, say
$c_2 = -8.5$, than the theoretically calculated one ($c_2 = - 4.68$). From
column 3 of table 4.3 it is seen that this gives a more satisfactory
behaviour for χ_{n^*} for the lowest densities. This might justify a re-
examination of the diagrams contributing to c_2 and their computation.

For the velocity autocorrelation function at low densities, some
examples are given in fig. 4.6 for densities up to $n^* = 0.0\overset{\sim}{2}$. These
functions deviate by a small amount from the Boltzmann result $\phi_B(s)$
[see (2.45)], therefore the difference $\phi(s) - \phi_B(s)$ is shown. In repre-
senting the data points by lines no smoothing was involved. For times

Table 4.3. Comparison of the experimental diffusion coefficient $v\sigma/D_e$ with the series expansion (2.25): $\chi_{n*} = (v\sigma/D_e - v\sigma/D)/\sigma_D(v\sigma/D_e)^2$, where σ_D is the standard deviation in $D_e/v\sigma$. In column 2 the coefficients in $v\sigma/D$ have been chosen according to (2.26). In column 3 the value $c_2 = -8.5$ has been used rather than -4.68.

$n*$	χ_{n*} $c_2 = -4.68$	χ_{n*} $c_2 = -8.5$
0.003	-0.55	0.95
0.004	-1.79	0.66
0.005	-3.87	0.49
0.010	-7.95	-0.84
0.015	-7.99	1.61
0.020	-13.94	-1.57
0.030	-8.21	-1.72
0.040	-5.71	2.88
0.050	-7.90	2.91
0.060	-1.73	4.48
0.070	-3.32	3.13
0.080	0.18	7.18
0.090	2.05	7.90
0.100	3.95	9.86

$s > 6$ an enlarged scale is used to give an idea of the influence of the cutoff at $s = 10$ or $s = 15$ on the values of $D_e/v\sigma$ listed in column 8 of table 4.1. For a number of points, error bars are given. It should be noted that for times of the order $s = 10$ no substantial contribution to the diffusion coefficient can be expected for the densities shown.

For the investigation of the asymptotic behaviour for long times the function $\phi(s) - \phi_B(s)$ has also been used. For low densities the contribution due to the ring diagrams is dominant. From these diagrams the asymptotic expression $\phi_A(s)$ has been derived [see (2.46)]. To improve the statistics,
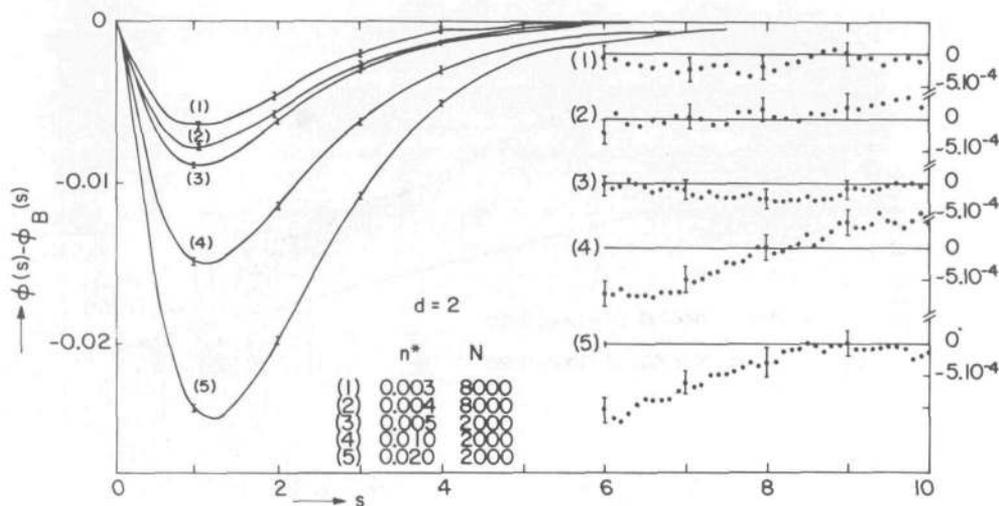
*Fig. 4.6. The difference of the experimental velocity autocorrelation
function φ(s) and the Boltzmann result φ_B(s) for five of the
low densities (lines). In drawing the lines no smoothing was
involved. The tail for s > 6 has been given on a four times
larger scale (dots).*

averages over the lowest-densities results up to $n^* = 0.02$ have been taken,
including a weight factor $1/n^*$ (since $\phi_A(s)$ is linear in the density).
Two averages have been computed this way: one for results with time in-
crement $h = 0.1$ [dots in fig 4.7] and the other one with $h = 0.15$ [crosses].
The resulting data are compared in fig 4.7 with $\phi_A(s)/n^*$ on a log-log scale.
From the comparison one can state that for times $s < 9$ the asymptotic be-
haviour as predicted by Ernst and Weyland has not yet set in. For larger
times the data do not disagree with the asymptotic expression, but in
this region the values are too small compared to the error bars to allow
for a more specific conclusion. The time integral over $\phi_A(s)$ for large
s is finite, in contrast to the moving-hard-disks case studied by
Alder and Wainwright[4.2], and would contribute only a fraction to the
diffusion coefficient for s > 10 of 3×10^{-9} for $n^* = 0.005$ and of
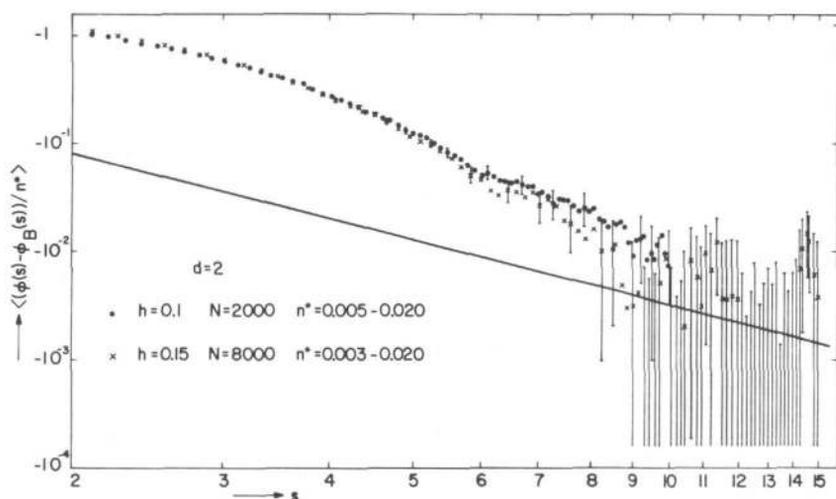6×10^{-7} for $n^* = 0.02$.

Fig. 4.7. The function $\phi(s) - \phi_B(s)$, averaged over several densities with
weight factor $1/n^*$, plotted on a log-log scale. The dots repre-
sent the average for $h = 0.1$, $N = 2000$ and the crosses the one
for $h = 0.15$, $N = 8000$. The straight line represents the corres-
ponding asymptotic expression $\phi_A(s)/n^* = -1/(\pi s^2)$.

For higher densities $\phi(s)$ is significantly different from zero even
for $s > 10$. Therefore, $\phi(s)$ has been calculated for larger values of s as
well. In fig 4.8 $\phi(s)$ is shown for 3 densities and the tails are shown on
an enlarged scale. In fig. 4.9 the corresponding mean square displacement
$\Delta(s)$ is shown. It has been multiplied by n^{*2} to arrive at a suitable scale:
one factor n^* for the reduction of the time axis by τ and a second factor
n^* for the linear term in the series expansion of $v\sigma/D$. It is clear that for
higher densities one has to wait longer before $\Delta(s)$ becomes linear. For
$n^* = 0.3$ it is doubtful whether it becomes linear at all. The explanation
is that at high densities it becomes very likely that scatterers in a
configuration form more or less closed pockets from which the moving
particle cannot escape or at least not within a reasonable short time. It
has not been possible to determine the percolation limit, i.e. a critical
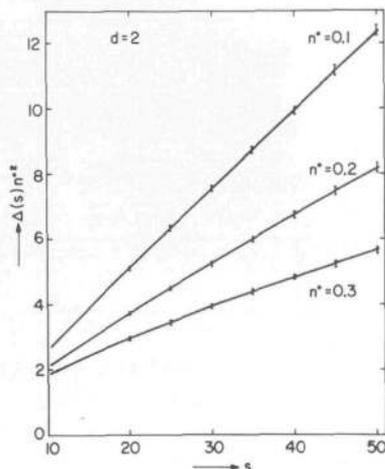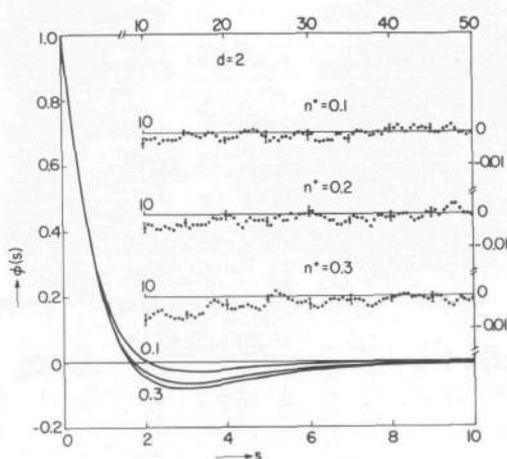density n^*_c, above which no diffusion is possible anymore.

Fig. 4.8. *The velocity autocorrelation function* $\phi(s)$ *for* $s < 10$ *has the smallest negative value for* $n^* = 0.1$ *and the largest one for* $n^* = 0.3$ *(lines). The statistical error is slightly larger than the line thickness. The tail for* $10 < s < 50$ *is given for the same three densities on an enlarged scale (dots).*

Fig. 4.9. *The reduced mean square displacement* $\Delta(s)n^{*^2}$ *for three densities starting with* $s = 10$. *The linear behaviour sets in for a larger time the higher the density.*

4.2. Three-dimensional Lorentz gas

The calculations performed for the three-dimensional Lorentz gas are much less extensive than for the two-dimensional case. From (2.27) it can be derived that the evidence for logarithmic terms in the density expansion for the inverse diffusion coefficient is much harder to obtain in three dimensions than in two dimensions. Therefore, having obtained some results (cases with N = 100 in table 4.4) showing good agreement with the first two terms in the expansion it was decided to spend no more time on the three-dimensional case. Later on some more extensive computations (cases with N = 2000 in table 4.4) have been performed for the study of the non-

Table 4.4. *Characteristic parameters and results for the 3-dimensional Lorentz gas*

1	2	3	4	5	6	7	8	9	10	11	12
n^*	N	N_c	$N_f N_c$ (10^6)	τ_e/τ	τ_N/τ	η_e^{-1}	χ^2	$D_e/v\sigma$	s_x	$D_e/v\sigma$	s_n, s_x
0.01	2000	480	0.96	0.999(1)	1.000	0.998(1)	1.19	10.55(11)	40	10.52(10)	40,100
0.05	2000	100	1	1.001(2)	1.000	1.000(1)	1.09	1.98(2)	50	1.97(2)	50,100
0.05	100	100	0.15	1.004(5)	0.998			2.02(7)	50	2.04(6)	45,50
0.10	2000	500	1	0.998(1)	1.000	0.998(1)	1.23	0.902(8)	60	0.895(7)	60,100
0.10	100	20	0.15	0.972(7)	0.996			0.93(3)	50	0.93(3)	45,50
0.15	100	20	0.15	0.95(1)	0.994			0.53(2)	50	0.54(2)	45,50
0.20	2000	500	1	1.001(2)	1.000	1.000(1)	1.05	0.379(4)	60	0.377(4)	60,100
0.20	100	20	0.15	1.02(2)	0.992			0.41(3)	50	0.40(3)	45,50
0.25	100	20	0.15	0.97(2)	0.990			0.28(1)	50	0.28(1)	45,50
0.30	2000	500	1	1.003(2)	0.999	1.002(1)	1.16	0.198(2)	60	0.198(2)	60,100
0.30	100	20	0.15	1.02(2)	0.987			0.20(1)	50	0.21(1)	45,50
0.35	100	20	0.15	1.03(3)	0.985			0.16(1)	50	0.16(1)	45,50
0.40	2000	500	1	1.008(3)	0.999	1.006(1)	1.07	0.108(2)	70	0.105(2)	70,100
0.40	100	20	0.15	1.00(3)	0.983			0.115(5)	50	0.115(5)	45,50
0.60	2000	2000	1	1.045(6)	0.999	1.040(2)	2.66	0.0298(8)	90	0.0299(6)	90,100
0.60	alternative			0.990(8)	0.999	0.991(1)	1.16				
0.80	2000	2000	1	1.095(8)	0.998	1.084(2)	4.34	0.0102(5)	90	0.0101(4)	90,100
0.80	alternative			0.998(8)	0.998	0.994(1)	1.06				

gaussian behaviour of Van Hove's self correlation function which can be related to the asymptotic behaviour of the velocity autocorrelation function[4.3]. However the unfavorable ratio between the magnitude of these non-gaussian correlations and the statistical accuracy obtained prevented us from presenting these results here.

In table 4.4 the results for the three-dimensional case are presented. This table has the same structure as table 4.1, except for one column which has been added (column 6). The values of the reduced Boltzmann mean free time for a finite system, τ_N/τ, are given in this column, since the deviation from the infinite-system value is not negligible in all cases.

At low densities, like in the two-dimensional case, τ_e/τ is in good agreement with the theoretical value 1, or rather τ_N/τ. For high densities τ_e/τ is significantly too high, the alternative average τ'_e/τ giving satisfactory results. The results on the free-times distribution, characterized by η_e^{-1} and χ^2, confirm this behaviour for the cases the distribution has been determined. The fitted value η_e^{-1} is in good agreement with τ_e/τ and χ^2 shows only large deviations from 1 for the straightforward average at high densities.

The diffusion coefficients $D_e/v\sigma$ shown in column 9 (table 4.4) have been obtained by integrating the velocity autocorrelation function. They are in good agreement with the ones obtained from the mean square displacement given in column 11. For the situations with $N = 100$ the velocity autocorrelation function has been determined in 100 equidistant points with a time increment $h = 0.1$ and in addition to these for larger times in 80 points with a time increment $h = 0.5$. For the situations with $N = 2000$ both the time increments have been doubled: giving $h = 0.2$ and $h = 1.0$ respectively. It should be noted that the upper bound s_x (column 10) for $n^* = 0.6$ and $n^* = 0.8$ may be too small or even does not exist, which would mean that diffusion is not possible at these high densities.

In fig. 4.10 the inverted experimental diffusion coefficients are given as a function of density; the dots represent results for the $N = 2000$ systems and the crosses some of the results for the $N = 100$
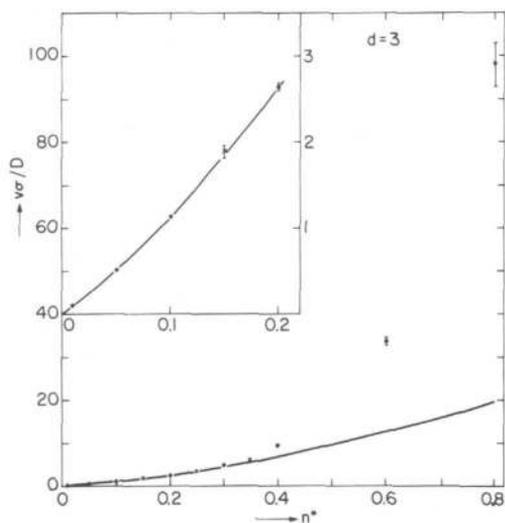
Fig. 4.10. *The experimental inverse diffusion coefficient as a function of the density for the 3-dimensional case with N = 2000 (dots) and N = 100 (crosses). The sum of the first three terms in the density expansion, $v\sigma/D = b_1 n^* + b_2 n^{*2} + b_3' n^{*3} \ln n^*$, is presented by the line. For low densities the data are shown on an enlarged scale.*

systems. Error bars have been omitted when they were smaller than the symbols used. For low densities up to $n^* = 0.25$ the agreement with the full line representing the first few terms of the density expansion (2.27) is very good. Dividing $v\sigma/D_e$ by n^* gives in fig. 4.11 a nice reproduction of the Boltzmann contribution $b_1 = 3\pi$ (dashed line) going to $n^* = 0$ and the data agree reasonably with the remaining terms of the series expansion $b_2 n^* + b_3' n^{*2} \ln n^*$(full line). Substracting the Boltzmann contribution and dividing once more by the density gives the results as shown in fig. 4.12. The full line represents $b_2 + b_3' n^* \ln n^*$. The fact that this line hardly deviates from a constant illustrates the smallness of the logarithmic term. The agreement between the data at low densities and the remaining part of the series expansion is not so good on this scale. Although the
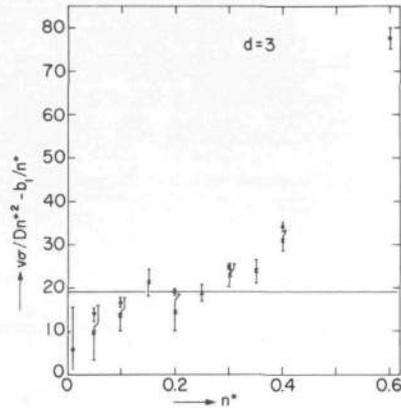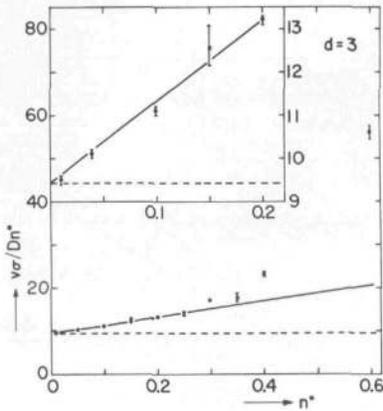
Fig. 4.11. Comparison of $v\sigma/D_e n^*$ [dots ($N = 2000$) and crosses ($N = 100$)]
with the Boltzmann term $b_1 = 3\pi$ (dashed line) and with
$b_1 + b_2 n^* + b_3' n^{*2} \ln n^*$ (full line).

Fig. 4.12. Comparison of $(v\sigma/D_e n^* - b_1)/n^*$ [dots ($N = 2000$) and crosses
($N = 100$)] with the remaining terms $b_2 + b_3' n^* \ln n^*$ (line).

error bars are large, the data show preference for a lower value of b_2.

The velocity autocorrelation function $\phi(s)$ is shown for some densi-
ties (situation with $N = 2000$) in fig. 4.13, the error bars are smaller
than the thickness of the drawn lines. The tails up to 100 mean free times
are shown on an enlarged scale (dots). The corresponding mean square dis-
placements are given in fig. 4.14. For every tenth point the error bar is
given, whenever it is larger than the thickness of the line drawn through
the data. It is seen that for the high density $n^* = 0.8$ $\Delta(s)$ does not be-
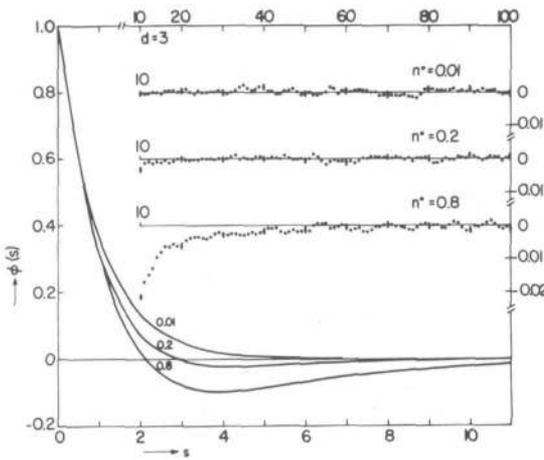come linear before $s = 100$.

Fig. 4.13. *The velocity autocorrelation function* $\phi(s)$ *for* $s < 11$ *for three densities (lines). The tail for* $10 < s < 100$ *is given for the same densities on an enlarged scale (dots).*
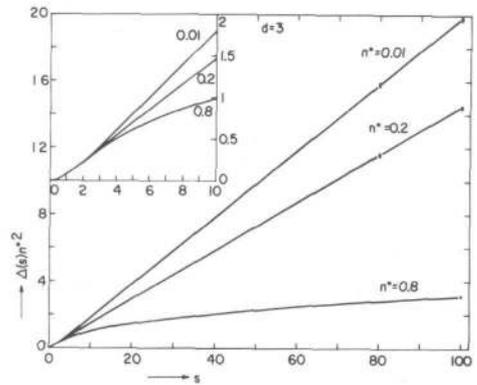
Fig. 4.14. *The reduced mean square displacement* $\Delta(s)n*^2$ *for three densities.*

4.3. Results on the N-dependence

Calculations concerning the dependence of the properties of the Lorentz gas on the number of scatterers N in the system, still employing periodic boundary conditions, were set up to find values of N for which the system is indistinguishable, within the limits of the statistical accuracy, from an infinite one. The strategy is to start with N = 1 and to increase N until the results are seen to converge. In section 2.4 it has been argued that finite-size effects will be the more serious the lower the density.

In the calculations on the N-dependence the number of collisions performed in each configuration is kept constant (see table 4.5). Therefore, the number of correlation sequences N_f fluctuates somewhat and so does the total number of correlation sequences $N_f N_c$ used in the averaging

procedure. For N = 1 there is no need to generate configurations with a different position of the scattering centre since the periodic boundary conditions always give a perfect lattice. This lattice breaks up into closed pockets for densities $n^* > 0.25$ in two dimensions and $n^* > \sqrt{2}/4 = 0.35$ in three dimensions. The distribution function of the free times $q_e(s_k)$

Table 4.5. N-dependence in two and three dimensions. In all cases $N_c = 100$.

1 n^*	2 N	3 $N_f N_c$ (10^5)	4 τ_e/τ	5 τ_N/τ	6 χ^2 $(\eta=1)$	7 $D_e/v\sigma$ $(s_x=50)$
			d = 2			
0.1	1	1.0	0.688(3)	0.686	1959	2.26(15)
0.1	2	1.2	0.884(24)	0.843	315	2.62(26)
0.1	4	1.4	0.948(21)	0.921	75	2.10(13)
0.1	8	1.5	0.989(17)	0.961	22	1.94(8)
0.1	25	1.5	0.983(10)	0.987	3.6	1.21(6)
0.1	50	1.5	0.995(7)	0.994	1.7	1.26(5)
0.01	1	1.4	0.965(7)	0.969	591	39(5)
0.01	2	1.5	0.992(11)	0.984	112	37(3)
0.01	4	1.5	0.989(9)	0.992	63	26(2)
0.01	8	1.5	0.999(8)	0.996	26	33(4)
0.01	25	1.5	0.999(4)	0.999	5.3	20(1)
0.01	50	1.5	0.993(4)	0.999	2.6	18(1)
			d = 3			
0.05	1	1.2	0.797(4)	0.791	376	2.83(25)
0.05	2	1.3	0.911(14)	0.895	99	3.62(42)
0.05	4	1.4	0.964(11)	0.948	31	2.32(10)
0.05	8	1.5	0.979(11)	0.974	11	2.54(25)
0.05	25	1.5	0.987(8)	0.992	2.5	2.00(7)
0.05	50	1.5	0.989(5)	0.996	1.5	2.03(6)

is very peculiar for N = 1. It was found to consist of a number of isolated peaks corresponding to free times between nearest neighbours, next-nearest neighbours and so on in the lattice formed by the periodic boundary condi-

tions. Beyond a certain time, which varies with the density, the peaks get connected.

For the two-dimensional case an intermediate density $n^* = 0.1$ is discussed first. In fig 4.15 the free-times distribution $q_e(s_k)$ is shown for some values of N. The significant peaks are easily identified as due to nearest, next-nearest and higher order periodic images of the scatterers. The deviations of the experimental mean free time τ_e/τ from 1 are very large but in very good agreement with τ_N/τ (columns 4 and 5 of table 4.5). The decrease of χ^2, calculated for $q_e(s_k)$ with respect to $\hat{Q}(s_k; \eta=1)$
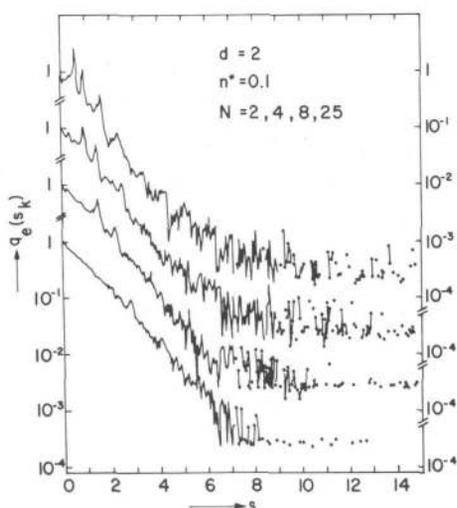

Fig. 4.15. The frequency distribution $q_e(s_k)$ for $d = 2$ and $n^* = 0.1$ with increasing N going downwards. Lines have been drawn through the data except for intervals which had zero intensity.
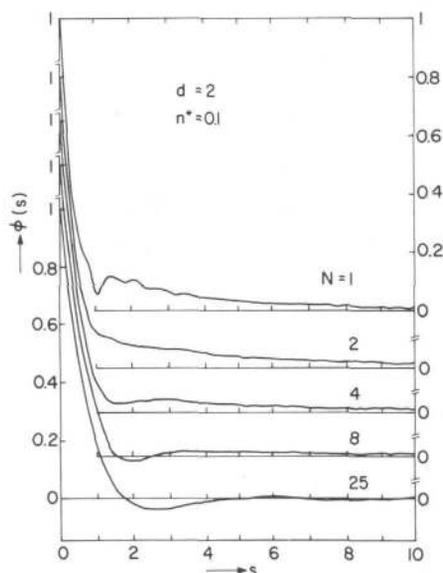
Fig. 4.16. The velocity autocorrelation function $\phi(s)$ for $d = 2$ and $n^* = 0.1$. The positive tail for small N is clearly demonstrated (although the behaviour for $10 < s < 50$ is not shown here).

in eq. (4.1), becomes considerable with increasing N (column 6 in table 4.5).

The diffusion coefficient $D_e/v\sigma$, obtained from integration of $\phi(s)$ with a maximum time $s_x = 50$, is much too large for small N (last column of table 4.5). It appears that lack of randomness in the system favours diffusion for densities that are not too high. This means that the event of repeated travelling across the system without collisions is dominant. This is also demonstrated in fig. 4.16 by the behaviour of $\phi(s)$. This function decreases relatively slowly for small N and has a long positive tail which was observed to be significantly different from zero at $s = 50$ for $N = 1$. For $N = 25$ it approaches its asymptotic behaviour, which can also be concluded from the values of $D_e/v\sigma$ in table 4.5 and the cases with $N = 500$ and $N = 2000$ for $n^* = 0.1$ in table 4.1.

The other density studied in two dimensions is $n^* = 0.01$ and this is a rather low one (table 4.5). The limiting value of $D_e/v\sigma$ is obtained for larger values of N. The system with $N = 50$ is probably still too small although this cannot be concluded from a calculation with this statistical accuracy. More extensive calculations gave $N = 100$: $D_e/v\sigma = 18.0 \pm 0.2$, $N = 500$: $D_e/v\sigma = 17.7 \pm 0.1$, $N = 2000$: $D_e/v\sigma = 17.77 \pm 0.03$ and $N = 8000$: $D_e/v\sigma = 17.80 \pm 0.02$.

From these results it can be concluded that the systems mentioned in table 4.1 are large enough to be free of significant finite-size effects. This is confirmed by the fact that results on the diffusion coefficient for different N at the same density, e.g. for $n^* = 0.005$ with $N = 2000$ and $N = 8000$, show no significant systematic differences.

In the three-dimensional case the N-dependence of one of the lowest densities mentioned in section 4.2, $n^* = 0.05$, has been investigated. Here too, τ_e/τ is considerably smaller than 1, but it is in reasonable agreement with τ_N/τ (table 4.5). For $N = 25$, $D_e/v\sigma$ seems to have reached its asymptotic value. So the systems with $N = 100$ in table 4.4 are sufficiently large to make finite-size effects neglectable compared to the obtained statistical accuracy. This is also confirmed by the data from the $N = 2000$ systems at the respective densities. However, this is rather surprising in view of the f values calculated in section 2.4. Apparently, travelling once across the system without collisions is less harmful in the 3-dimensional than in the 2-dimensional case. This was also indicated

by the values of the geometrical factor f_g given in section 2.4.

References

4.1) Wood, W.W., private communication

4.2) Alder, B.J. and Wainwright, T.E., Phys. Rev. <u>A1</u> (1970) 18

4.3) Wood. W.W., (1974) in Fundamental Problems in Statistical Mechanics III
Ed. E.G.D. Cohen, North-Holland Publishing Company, Amsterdam 1975

5. CONCLUSIONS

Qualitative evidence has been obtained for a logarithmic term in the density expansion of the inverse diffusion coefficient for the two-dimensional Lorentz gas. As the arguments used by Van Leeuwen and Weyland to arrive at the expression for the logarithmic terms are similar to those used for other systems, the evidence found in this case sustains the occurrence of logarithmic terms in other, and more realistic, systems.

The computations are not conclusive with respect to the power-like decay of the velocity autocorrelation function. They do show that the asymptotic behaviour is not dominant before 9 mean free times, even for low densities. This makes it very hard to verify this behaviour.

For the three-dimensional case the results show reasonable agreement for the diffusion coefficient with the predicted density expansion and thus confirm the expectation that evidence for logarithmic terms in three dimensions is very hard to obtain.

As regards the mean free time and distribution of free times good agreement has been observed between theoretical and experimental results, if use is made of a more appropriate alternative average described in this thesis.

APPENDIX: The joint distribution of the first and second free time for the two-dimensional case.

The derivation given in this appendix is a modification of a calculation performed by Wood[2.5] for the overlapping Ehrenfest wind-tree model. Consider a two-dimensional Lorentz gas of N point-scatterers in a volume Ω, with density $n = N/\Omega$, and a moving particle (disk) of radius σ. Let $t_1(x,R^N)$ denote the time until the first collision and $t_2(x,R^N)$ the time between the first and the second collision, starting with initial condition $x = (\vec{p},\vec{q})$ of the moving particle, of which the trajectory in phase space is further completely determined by the configuration of scatterers R^N. The joint distribution $P_2(t_1,t_2)$ to be calculated is defined by

$$P_2(t_1,t_2) = < \delta [t_1 - t_1(x,R^N)] \ \delta [t_2 - t_2(x,R^N)] > , \qquad (A.1)$$

where the average has to be performed over all possible values of $\vec{q}$ and R^N and over all possible directions of the velocity $\vec{v}(= \vec{p}/m)$. This average can be reduced without loss of generality to an average over R^N alone.

For the joint distribution four factors are important, as will be discussed for the simple case shown in fig. A.1. Here L_1 is the initial position (of the centre) of the moving particle, L the position at the first collision, L_2 the position at the second collision and ϕ is the scattering angle for the first collision; the distances L_1B, LJ and L_2E are all equal to σ and furthermore one has $L_1L = vt_1$ and $LL_2 = vt_2$.

1) The probability f_1dt_1 that one of the scatterers gives a first free time between t_1 and t_1+dt_1 is equal to the product of the density $N/(\Omega - \pi\sigma^2)$ of the scatterers, corrected for the volume of the moving particle, and the area $2\sigma vdt_1$ of width vdt_1 along CDK. Because of symmetry one needs to consider only the part CD, taking a factor 2 into account. So one has $f_1dt_1 = 2\sigma vdt_1 N/(\Omega - \pi\sigma^2)$.

Fig. A.1. Case A with conditions IK > HK, GM > HM.
$$\Omega_A = ABCDJEFGHI, \quad \ell_A = 2, \quad L_1B = \sigma, \quad L_1L = vt_1 \text{ and } LL_2 = vt_2.$$

2) The probability $f_\phi d\phi$ that the angle between the velocities before and after the first collision is between ϕ and $\phi+d\phi$ is proportional to dy, with y varying from 0 to σ along DC. Taking L' as the position of the scatterer and requiring that the angle of incidence equals the angle of reflection, one obtains for the relation between y and ϕ the result $y = \sigma \cos \frac{1}{2}\phi$. Thus, for $0 \leqslant \phi \leqslant \pi$ one has $f_\phi d\phi = \frac{1}{2} \sin \frac{1}{2}\phi \, d\phi$, where the factor σ has been dropped because of normalization.

3) The probability $f_2 dt_2$ that one of the scatterers gives a second free time between t_2 and t_2+dt_2 is equal to the product of the density $(N - 1)/(\Omega - \pi\sigma^2)$ of the remaining scatterers and the area $\ell_\alpha \sigma v dt_2$ of width $v dt_2$ along EFG. In the case shown in fig. A.1 one has $\ell_\alpha = 2$, but in other cases ℓ_α may differ from that value; e.g. when for small t_2 it may occur that MG < MH. This results in a factor $f_2 dt_2 = \ell_\alpha \sigma v dt_2 (N-1)/(\Omega-\pi\sigma^2)$.

4) The probability f_Ω that the collisions at time t_1 and t_2 do take place is equal to the probability that none of the remaining scatterers lies inside an area Ω_α. In fig. A.1. this area is enclosed by the contour ABCDJEFGHI. The expression for Ω_α depends on the case considered. This gives obviously $f_\Omega = \{ (\Omega - \Omega_\alpha)/(\Omega - \pi\sigma^2) \}^{N-2}$. Combination of the four

factors gives for the joint distribution

$$P_2(t_1,t_2)dt_1dt_2 = \frac{N(N-1)2\sigma^2 v^2}{(\Omega - \pi\sigma^2)^2} \, dt_1dt_2 \int_0^\pi \ell_\alpha\{\frac{\Omega-\Omega_\alpha}{\Omega-\pi\sigma^2}\}^{N-2} \tfrac{1}{2}\sin\tfrac{1}{2}\phi \, d\phi,$$

(A.2)

which in the limit $N \to \infty$ simplifies to

$$P_2(t_1,t_2)dt_1dt_2 = 2n^2\sigma^2 v^2 dt_1dt_2 \int_0^\pi \tfrac{1}{2}\ell_\alpha(\sin\tfrac{1}{2}\phi)\{\exp - n(\Omega_\alpha-\pi\sigma^2)\}d\phi,$$

(A.3)

where ℓ_α and Ω_α are functions of t_1, t_2 and ϕ.

For the calculation of Ω_α and ℓ_α different cases, as shown in fig. A.2, have to be considered. The dashed-dotted lines denote boundaries
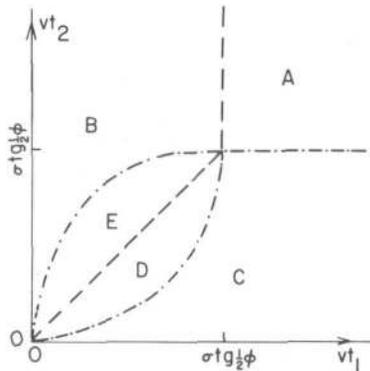
Fig. A.2. Different cases in the calculation of $P_2(t_1,t_2)$, see text.

on which the expressions of both Ω_α and ℓ_α change. On the dashed lines only the expression for Ω_α changes. The envelop of region E + D is drawn for the case $\phi = \pi/2$, for other values of ϕ this region only changes quantitatively. The different cases will now be considered in detail.

Case A. (see fig. A.1). The conditions for this simplest case are

$vt_1 > HK$ and $vt_2 > MH$, which can be reduced to

$$vt_1 > \sigma tg\tfrac{1}{2}\phi, \qquad vt_2 > \sigma tg\tfrac{1}{2}\phi. \tag{A.4}$$

The expression for the area Ω_A is easily obtained by correcting for the overlap of the area's ABCMKI and FGMKJE. The result is

$$\Omega_A = \pi\sigma^2 + 2\sigma vt_1 + 2\sigma vt_2 - \sigma^2 \{ tg\tfrac{1}{2}\phi - \tfrac{1}{2}\phi \} . \tag{A.5}$$

For ℓ_A one has as mentioned above

$$\ell_A = 2 . \tag{A.6}$$

In fig. A.1 a situation for $\phi > \tfrac{1}{2}\pi$ has been drawn, for $\phi < \tfrac{1}{2}\pi$ one obtains in a similar way the same expressions for Ω_A and ℓ_A. This will hold true for all cases to be discussed.

Case B. (see fig. A.3). The conditions for this case are $vt_1 < HK$ and $vt_2 > MS$. It is obvious that the condition on vt_2 can be taken to
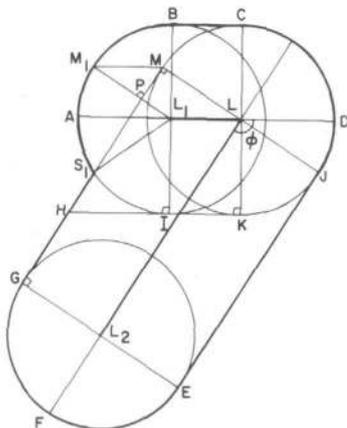
Fig. A.3. Case B with conditions $IK < HK$, $GM > S_1M$.
$\Omega_B = ABCDJEFGS_1$, $\ell_B = 2$, $L_1B = \sigma$, $L_1L = vt_1$ and $LL_2 = vt_2$.

be weaker than $vt_2 > MH$, what one might expect from case A. It is convenient for the evaluation of Ω_B to choose a point M_1 such that

MM_1 // CB; then one also has M_1L_1 // ML. By evaluating now the areas M_1MCB, M_1MP and M_1PS_1A one obtains

$$\Omega_B = \pi\sigma^2 + 2\sigma vt_2 + \sigma vt_1 (1 + \cos\phi) - \tfrac{1}{2}(vt_1)^2 \sin\phi\cos\phi$$

$$+ \tfrac{1}{2}\sigma^2 \arccos [1 - (vt_1/\sigma) \sin\phi] - \tfrac{1}{2}(\sigma - vt_1 \sin\phi) [2\sigma vt_1 \sin\phi - (vt_1 \sin\phi)^2]^{\tfrac{1}{2}} .$$ (A.7)

It is obvious that one has again

$$\ell_B = 2 .$$ (A.8)

The explicit expression for the conditions on case B reads

$$vt_1 < \sigma tg\tfrac{1}{2}\phi, \quad vt_2 > [2\sigma vt_1 \sin\phi - (vt_1 \sin\phi)^2]^{\tfrac{1}{2}} - vt_1 \cos\phi .$$ (A.9)

Case C. (see fig. A.4). The conditions for this case are $vt_1 > KS_2$ and $vt_2 < HM$. This case is identical to case B after interchanging the
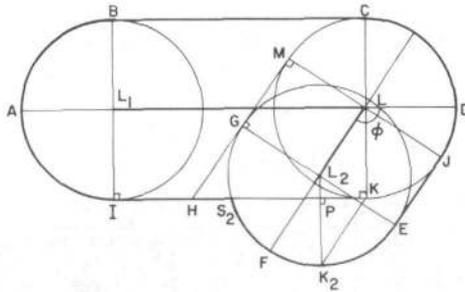
Fig. A.4. Case C with conditions GM < HM, IK > S_2K.
$\Omega_C = ABCDJEFS_2I$, ℓ_C = projection of arc S_2E onto GE, $L_1B = \sigma$,
$L_1L = vt_1$ and $LL_2 = vt_2$.

variables t_1 and t_2, except for the expresssion for ℓ_C. Here a point K_2 is chosen, KK_2 // JE. By calculating now the areas K_2KJE, K_2KP and

K_2PS_2F one finds

$$\Omega_C = \pi\sigma^2 + 2\sigma vt_1 + \sigma vt_2(1+\cos\phi) - \tfrac{1}{2}(vt_2)^2 \sin\phi\cos\phi \tag{A.10}$$

$$+ \tfrac{1}{2}\sigma^2 \arccos[1-(vt_2/\sigma)\cos\phi] - \tfrac{1}{2}(\sigma-vt_2\sin\phi)[2\sigma vt_2\sin\phi-(vt_2\sin\phi)^2]^{\tfrac{1}{2}}.$$

Because the arc GS_2 lies inside the region where no scatterers are allowed, the value of ℓ_C differs from two:

$$\ell_C = 1+[1-(vt_2/\sigma)\sin\phi]\cos\phi + [2(vt_2/\sigma)\sin\phi-(vt_2/\sigma)^2\sin^2\phi]^{\tfrac{1}{2}}\sin\phi . \tag{A.11}$$

The conditions on case C read in detail

$$vt_1 > [2\sigma vt_2\sin\phi-(vt_2\sin\phi)^2]^{\tfrac{1}{2}} - vt_2\cos\phi , \quad vt_2 < \sigma tg\tfrac{1}{2}\phi. \tag{A.12}$$

Case D. (see fig. A.5). The remaining region (see fig. A.2) is dealt with by considering, for convenience of the analysis as well as the numerical treatment, two more cases D and E. The whole region could be covered by any one of these cases. The boundary between the two corresponding areas is thus arbitrary and the line $vt_1 = vt_2$ has been chosen because of symmetry. For case D obviously the following conditions hold:

$$vt_2 < vt_1 < [2\sigma vt_2\sin\phi - (vt_2\sin\phi)^2]^{\tfrac{1}{2}} - vt_2\cos\phi . \tag{A.13}$$

The calculation of Ω_D is similar to that of Ω_C, except for the areas K_2PIU and UIS which lead to rather complicated expressions. The distance L_1L_2 will be denoted by

$$\ell_{12} = [(vt_1)^2 + (vt_2)^2 + 2vt_1vt_2\cos\phi]^{\tfrac{1}{2}} . \tag{A.14}$$

One finds then

$$\Omega_D = \pi\sigma^2 + 2\sigma vt_1 + \sigma vt_2(1+\cos\phi) - \tfrac{1}{2}(vt_2)^2 \sin\phi\cos\phi +$$

$$+ \tfrac{1}{2}\sigma^2\zeta - \tfrac{1}{2}(\sigma - vt_2\sin\phi)(vt_1 + vt_2\cos\phi) + \tfrac{1}{2}\sigma^2(\nu - \upsilon)$$

$$-\tfrac{1}{2}(\sigma^2 - 2\sigma vt_2\sin\phi + \ell_{12}^2)^{\tfrac{1}{2}} \ell_{12} \sin\rho\sin\nu/\sin(\rho + \xi) , \qquad (A.15)$$

where a number of auxiliary angles have been introduced (see also fig. A.5):

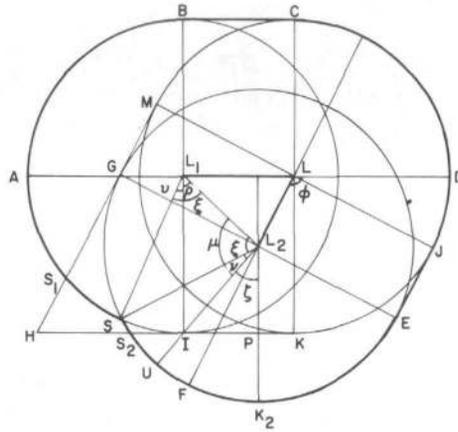Fig. A.5. *Case D with conditions* $IK < S_2K$, $IK > GM$.
$\Omega_D = ABCDJEFS$, $\ell_D = $ *projection of arc SE onto GE*, $L_1B = \sigma$,
$L_1L = vt_1$ *and* $LL_2 = vt_2$.

$$\zeta = \angle IL_2P = \text{arctg} (vt_1 + vt_2\cos\phi)/(\sigma - vt_2\sin\phi),$$

$$\nu = \mu - \xi ,$$

$$\upsilon = \xi - \rho , \qquad (A.16)$$

$$\mu = \angle IL_2L_1 = \arccos (\ell_{12}^2 - \sigma vt_2\sin\phi)/\ell_{12}'(\sigma^2 - 2\sigma vt_2\sin\phi + \ell_{12}^2)^{\tfrac{1}{2}},$$

$$\xi = \angle SL_2L_1 = \arccos \ell_{12}/2\sigma ,$$

$$\rho = \angle IL_1L_2 = \arccos vt_2 \sin\phi / \ell_{12}.$$

By evaluating the arc GS in this case, one finds for the set of allowed positions of scatterers along arc SE:

$$\ell_D = 1 + (vt_1/2\sigma)\sin\phi + (vt_1\cos\phi + vt_2)\{ \ell_{12}^{-2} - (4\sigma^2)^{-1}\}^{\frac{1}{2}} \qquad (A.17)$$

Case E. This case needs not to be discussed in detail. Ω_E can be obtained from Ω_D by interchanging vt_1 and vt_2. The expression for ℓ_E is identical to the one for ℓ_D. The conditions for this case read

$$vt_1 < vt_2 < [2\sigma vt_1 \sin\phi - (vt_1 \sin\phi)^2]^{\frac{1}{2}} - vt_1 \cos\phi . \qquad (A.18)$$

As a check on the expressions for the different cases it can be shown that they match on the boundaries. It is appropriate to reduce time with respect to the Boltzmann mean free time, as has been done in chapter 2. We define

$$s_1 = 2n\sigma vt_1 = t_1/\tau, \quad s_2 = 2n\sigma vt_2 = t_2/\tau \qquad (A.19)$$

and moreover a reduced volume Ω_α^* given by

$$\Omega_\alpha^* = n(\Omega_\alpha - \pi\sigma^2). \qquad (A.20)$$

Substituting (A.19) and (A.20) into (A.3) and taking into account the Jacobian of the transformation, one finds for the reduced joint distribution

$$P_2^* (s_1,s_2)ds_1 ds_2 = ds_1 ds_2 \int_0^\pi d\phi \; \tfrac{1}{4}\ell_\alpha \sin\tfrac{1}{2}\phi \; \exp - \Omega_\alpha^* . \qquad (A.21)$$

It should be noted that depending upon the pertaining values of s_1, s_2,

ϕ and n^* the correct expressions for Ω_α^* and ℓ_α have to be chosen from cases A until E.

The joint distribution $P_2^*(s_1,s_2)$ can be obtained from (A.21) by numerical integration over ϕ. The distribution of the first free time $P_{2,1}^*(s_1)$ can be obtained subsequently by numerical integration over s_2. This serves as a check on the whole procedure since this result should be identical to the result for $P(t)$, see (2.54). Numerical integration of $P_2^*(s_1,s_2)$ over s_1 gives the distribution of the second free time $P_{2,2}^*(s_2)$. Subsequent integration over s_2 gives another check, since the result should be equal to one because of normalization. For a number of densities the distribution of the second free time $P_{2,2}^*(s_2)$ is shown in fig. A.6, together with a pure exponential. The deviation form a pure exponential increases as a function of the density. For $s_2 = 0$ the distribution is independent of the density, in fact $P_{2,2}^*(0)$ can be evaluated exactly to give 1/3. In table A.1 the first moment $<s_2>$ of the distribution of the second free time $P_{2,2}^*(s_2)$ is given as a function of the density. The deviation of the

Table A.1. The average of the second free time $<s_2>$ as a function of the density (the time s_2 is reduced with respect to the Boltzmann mean free time τ).

n^*	$<s_2>$
0.005	1.02
0.01	1.03
0.02	1.05
0.05	1.10
0.1	1.14
0.2	1.21
0.5	1.31
1.0	1.37
10.	1.43

average of the second free time from the Boltzmann mean free time increases with density.

At the densities for which the numerical integration has been performed, the interval 0 to π for ϕ has been divided into 40 intervals.
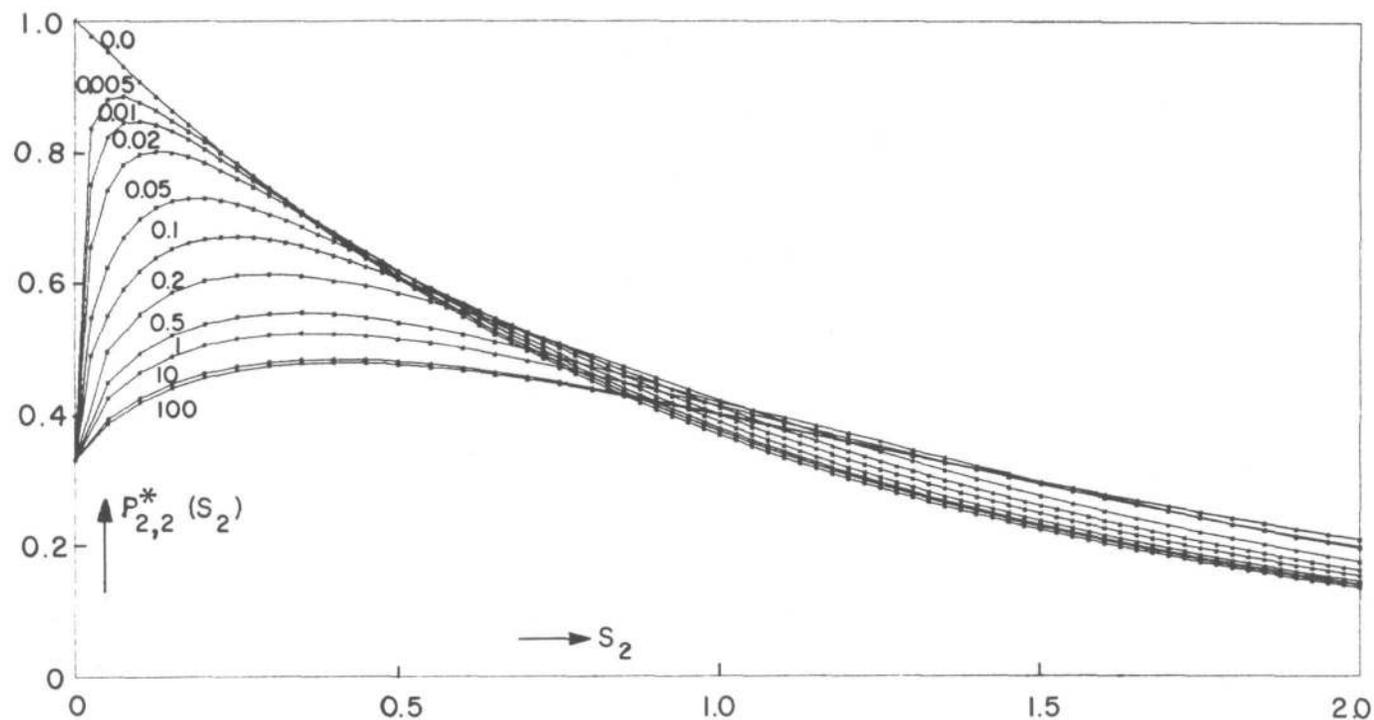
Fig. A.6. The distribution of the second free time $P_{2,2}^*(s_2)$ for a number of densities. For the density $n^* = 0$ the distribution is a pure exponential.

The maximum value for s_1 and s_2 used was 7.5; this range has been divided into 150 intervals for densities $n^* > 0.1$ and into 300 intervals for the lower ones. For all integrations the Simpson (3-point) rule has been used, giving an accuracy of better than 1%.

SUMMARY

The numerical study of the Lorentz gas has been undertaken as to obtain quasi-experimental data on the density dependence of the diffusion coefficient. Primarily the 2-dimensional case has been studied, for which the deviations from a pure power series in the density for the inverse diffusion coefficient are expected to be most dominant. In the 1-dimensional case there is no diffusion at all and for 3 dimensions the expected deviations are relatively small.

For a more substantial comparison of theory and experiment, two additional terms in the series expansion of the inverse diffusion coefficient have been calculated for the 2-dimensional case: the regular term of the same order in density as the dominant logarithmic term and the most important logarithmic term of one order higher in the density.

As a check on the computations, especially for the Monte-Carlo part of it, expressions have been derived for the distribution function of free times and for the mean free time.

For the computation of the static quantities (initial conditions) the crude Monte-Carlo method has been used. The time-dependent behaviour has been computed with the method of molecular dynamics (solving the equations of motion). For the Monte-Carlo method the generator of pseudo-random numbers is essential and its properties have been studied. In this respect the distribution function of free times appeared to be useful. Optimalization of the molecular-dynamics computations, especially dividing the system into sub-systems (cells), resulted in a considerable saving of computing time.

The computed diffusion coefficients for the 2-dimensional case at low densities are in good agreement with the predicted dominant logarithmic term. The contribution of the two terms calculated in addition to the ones already known is not quite satisfactory.

The dependence of the results on the size of the system has been investigated experimentally. However this investigation could be facilitated by using an expression describing the density dependence of finite-size effects. The influence of finite N on the cases reported is smaller than the statistical accuracy obtained.

SAMENVATTING

De numerieke studie van het lorentzgas is ondernomen teneinde quasi-experimentele gegevens te verkrijgen omtrent de dichtheidsafhankelijk-heid van de diffusiecoefficient. De aandacht is hierbij vooral gericht op het 2-dimensionale geval waar de verwachte afwijkingen van een zuivere machtreeks in de dichtheid voor de reciproke diffusiecoefficient het grootst zijn. In het 1-dimensionale geval is er geen diffusie en voor 3 dimensies zijn de verwachte afwijkingen gering.

Voor een meer solide vergelijking tussen theorie en experiment zijn twee extra termen in de reeksontwikkeling van de reciproke diffusiecoef-ficient berekend voor het 2-dimensionale geval: de reguliere term van de-zelfde orde in de dichtheid als de dominante logarithmische term en de belangrijkste logarithmische term van één orde hoger in de dichtheid.

Als toetsen voor de numerieke berekeningen, en vooral voor het monte-carlo aspect ervan, zijn uitdrukkingen afgeleid voor de verdelings-functie van de vrije weglengten en voor de gemiddelde vrije weglengte.

Voor de uitvoering van de numerieke berekeningen is voor de sta-tische grootheden de eenvoudige monte-carlomethode gebruikt en voor het tijdafhankelijk gedrag de methode van moleculaire dynamica. Voor de monte-carlomethode is aan de generator van pseudo-randomgetallen de no-dige aandacht besteed. De verdelingsfunctie van vrije weglengten blijkt in dit opzicht een nuttig hulpmiddel. Optimalisering van de moleculaire-dynamicaberekeningen, vooral de verdeling van het systeem in cellen, leidt tot een grote besparing van rekentijd.

De berekende diffusiecoefficienten voor het 2-dimensionale geval bij lage dichtheden zijn in goede overeenstemming met de voorspelde dominante logarithmische term. De bijdrage van de twee extra berekende termen vol-doet niet aan de verwachtingen.

De afhankelijkheid van de resultaten van de grootte van het systeem

is voornamelijk experimenteel onderzocht, zij het met behulp van een theoretische voorspelling voor de afhankelijkheid van de dichtheid. De invloed van eindige N voor de beschouwde gevallen is kleiner dan de bereikte statistische nauwkeurigheid.
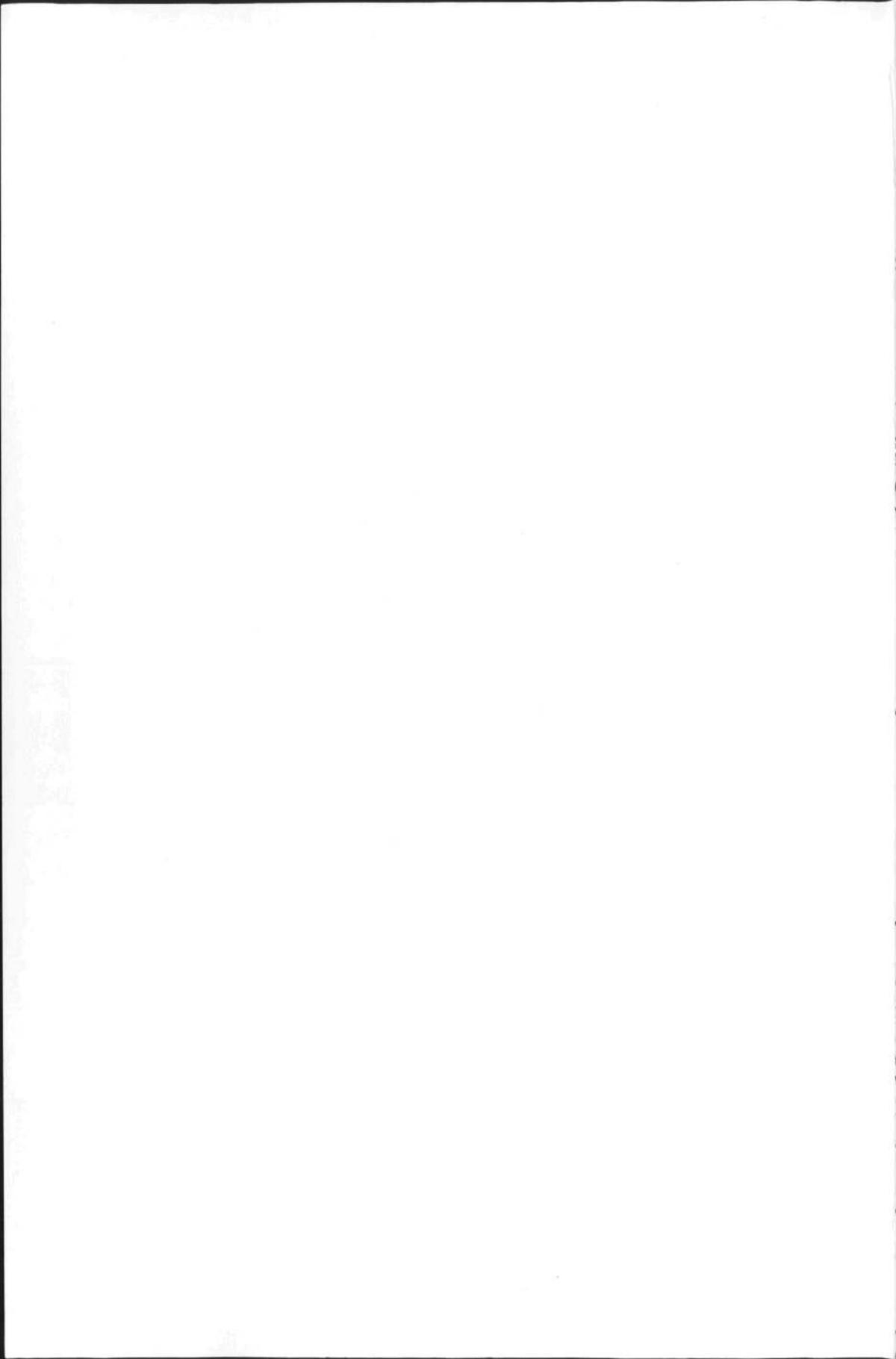
ACKNOWLEDGEMENTS

STELLINGEN

I

Als controle op de correcties van resultaten van neutronenverstrooiings-
experimenten is het aan te bevelen moleculaire-dynamicaberekeningen te
doen.

   C. Bruin en A. Hasman, Phys. Letters 33A (1970) 338

   A. Hasman en P. Zandveld, Phys. Letters 34A (1971) 112

II

De bewering dat simulaties in de fysica niet voorkomen is aanvechtbaar.

   C.A. van Peursen en S. Boendermaker, Intermediair 12e jaargang 3
   (1976) 25

III

Het model voor de smeltovergang van Briant en Burton heeft voor elke tem-
peratuur een 'ergodische potentiaal' in de faseruimte als men met behulp
van een markovproces middelt over het kanoniek ensemble.
Dit vermindert de relevantie van dit model voor de door hen onderzochte
smeltovergang van microclusters, waar voor lage temperaturen de fase-
ruimte niet ergodisch blijkt te zijn voor middelingen over het kanoniek
ensemble berekend met behulp van een markovproces.

   C.L. Briant en J.J. Burton, J. Chem. Phys. 63 (1975) 2045

IV

De introductie van een potentiaalbarrière met ruimtelijke uitgebreidheid
in het model voor de smeltovergang van Briant en Burton zal leiden tot
realistischer resultaten voor gemiddelden over het kanoniek ensemble.

C.L. Briant en J.J. Burton, J. Chem. Phys. 63 (1975) 2045

V

Het kan bewezen worden dat in een 1-dimensionaal roostergas bij constante
druk de dichtheid kleiner is naarmate de roosterconstante kleiner is.
Dezelfde relatie tussen dichtheid en roosterconstante geldt op de bodem
van een lineaire atmosfeer.

C. Bruin en A. Compagner, Physica 68 (1973) 171

VI

Wanneer de coefficient van zelfdiffusie op de juiste wijze met behulp van
de enskogtheorie berekend wordt, is er uitstekende overeenkomst met zo-
wel de experimentele waarde als die uit het computerexperiment.

C. Bruin, Phys. Letters 28A (1969) 778

VII

Voor de bewering van Cicotti en Jacucci dat hun methode voor simulatie van de
dynamische responsie van een systeem niet geschikt is voor effecten op
tamelijk lange tijden is hun argument voor het exponentiëel uiteengegaan
van trajectoriën in de faseruimte niet voldoende. De invloed van de grootte
van het uitwendige veld zal daartoe eerst onderzocht moeten worden.

G. Cicotti en G. Jacucci, Phys. Rev. Letters 35 (1975) 789
S.D. Stoddard en J. Ford, Phys. Rev. A8 (1973) 1504

VIII

Gezien het belang dat de afdeling Technische Natuurkunde hecht aan
fundamenteel onderzoek als onderdeel in de opleiding tot natuurkundig
ingenieur verdienen fysisch georienteerde computersimulaties in deze
opleiding een plaats.

IX

Programma's die terwille van de statistische nauwkeurigheid veel com-
putertijd vergen zouden, bij onvoldoende ruimte in de nachten gedurende
de werkweek, in het weekeinde gedraaid moeten kunnen worden. Berekeningen
van dit type vermeld in dit proefschrift hadden ruimschoots uitgevoerd
kunnen worden door de computer gedurende een half jaar tijdens de week-
einden niet uit te schakelen.

C. Bruin   Delft, 1 maart 1978